

THESIS FOR THE DEGREE OF DOCTOR OF PHILOSOPHY

Nonlinear Characterisation and Modelling of  
Microwave Semiconductor Devices

MATTIAS THORSELL



Microwave Electronics Laboratory  
Department of Microtechnology and Nanoscience (MC2)  
Chalmers University of Technology  
Göteborg, Sweden, 2011

# Nonlinear Characterisation and Modelling of Microwave Semiconductor Devices

MATTIAS THORSELL

© Mattias Thorsell, 2011

ISBN 978-91-7385-579-2

Doktorsavhandlingar vid Chalmers tekniska högskola  
Ny serie nr 3260  
ISSN 0346-718X

Technical report MC2-200  
ISSN 1652-0769

Microwave Electronics Laboratory  
Department of Microtechnology and Nanoscience (MC2)  
Chalmers University of Technology  
SE-412 96 Göteborg, Sweden  
Phone: +46 (0) 31 772 1000

Printed by Chalmers Reproservice  
Göteborg, Sweden 2011

# Abstract

There is an increasing need for more accurate models taking into account the nonlinearities and memory effects of microwave transistors. The memory effects are especially important for transistor technologies suffering from relatively large low frequency dispersion, such as GaN based HEMTs. Nonlinear measurement systems are today available off-the-shelf, but the use of them is still limited. It is therefore important to demonstrate the possibilities these new systems brings to the device characterisation and modelling community. This thesis deals with electrothermal characterisation and modelling of GaN based HEMTs, and also development and utilisation of new nonlinear measurement systems.

The electrothermal properties of the AlGaIn/GaN heterostructure were characterised, and it was shown that a thermal response is present up to 100 MHz. Moreover, a new characterisation method, making use of nonlinear measurements, allowed for isothermal measurements of the current transport through the access resistances of a GaN based HEMT. A new current transport model was proposed to correctly reproduce the isothermal IV characteristics. Furthermore, the temperature dependence of the high frequency noise was characterised, showing that the major limiting factors for the low noise performance were the access resistances. The combination of high power and low noise makes the GaN based HEMT suitable for monolithically integrated GaN based transceiver front-ends. The first steps toward a transceiver were taken by designing and manufacturing a GaN based receiver front-end consisting of an SPDT switch and an LNA.

A new fast multi harmonic active load-pull system was developed, with waveform acquisition capabilities. The speed of the load-pull system was increased by the use of an improved optimisation routine for presenting the wanted load impedances. The load-pull system was capable of presenting dynamically varying load impedances to a transistor, enabling faster device characterisation without the need to build complete amplifiers. The system was also used to characterise the nonlinear distortion in SiC varactors. It was shown that the nonlinear distortion increases the losses, and hence a new general Q-factor description was proposed. Furthermore, a new characterisation method was proposed which enabled the study of memory effects in transistors driven by modulated signals.

**Keywords:** active load-pull, AlGaIn/GaN HEMT, noise measurement, noise modelling, nonlinear measurement, nonlinear modelling, thermal characterisation



# List of publications

## Appended publications

This thesis is based on work contained in the following papers:

- [A] M. Thorsell, K. Andersson, H. Hjelmgren, and N. Rorsman "Electrothermal Access Resistance Model for GaN Based HEMTs," *IEEE Transactions on Electron Devices*, vol. 58, no. 2, pp. 466–472, February, 2011.
- [B] M. Thorsell, K. Andersson, M. Fagerlind, M. Södow, P.-Å. Nilsson, and N. Rorsman "Thermal Study of the High-Frequency Noise in GaN HEMTs," *IEEE Transactions on Microwave Theory and Techniques*, vol. 57, no. 1, pp. 19–26, January, 2009.
- [C] M. Thorsell, M. Fagerlind, K. Andersson, N. Billström, and N. Rorsman "An X-Band AlGaIn/GaN MMIC Receiver Front-End," *IEEE Microwave and Wireless Components Letters*, vol. 20, no. 1, pp. 55–57, January, 2010.
- [D] M. Thorsell, and K. Andersson "Fast Multi Harmonic Active Load-Pull System With Waveform Measurement Capabilities," to appear in *IEEE Transactions on Microwave Theory and Techniques*.
- [E] M. Thorsell, K. Andersson, and C. Fager "Characterization Setup for Device Level Dynamic Load Modulation Measurements," in *2009 IEEE MTT-S International Microwave Symposium Digest*, Boston, MA, USA, June, 2009.
- [F] M. Thorsell, K. Andersson, G. Pailloncy, and Y. Rolain "Extending the Best Linear Approximation to Characterize the Nonlinear Distortion in GaN HEMTs," to appear in *IEEE Transactions on Microwave Theory and Techniques*.
- [G] C. M. Andersson, M. Thorsell, and N. Rorsman "Nonlinear Characterization of Varactors for Tunable Networks by Active Source-Pull and Load-Pull," *IEEE Transactions on Microwave Theory and Techniques*, vol. 59, no. 7, pp. 1753–1760, July, 2011.

## Other publications

The following papers have been published but are not included in the thesis. Their content partially overlap with the appended papers or are out of the scope of this thesis.

- [a] M. Thorsell, K. Andersson, G. Pailloncy, and Y. Rolain "Using the Best Linear Approximation to Model the Nonlinear Behavior of Supply Modulated Amplifiers," in *6th European Microwave Integrated Circuits Conference*, Manchester, England, October, 2011.
- [b] K. Andersson, M. Thorsell, G. Pailloncy, and F. Verbeyst "Large-signal waveform acquisition of pulsed signals," in *41st European Microwave Conference*, Manchester, England, October, 2011.
- [c] M. Özen, C.M. Andersson, M. Thorsell, K. Andersson, N. Rorsman, C. Fager, M. Acar, M. P. van der Heijden, and R. Jos "High efficiency RF pulse width modulation with tunable load network class-E PA," in *2011 IEEE Wireless and Microwave Technology Conference*, Clearwater, FL, USA, April, 2011.
- [d] H. Otsuka, T. Oishi, K. Yamanaka, M. Thorsell, K. Andersson, A. Inoue, Y. Hirano, and I. Angelov "Semi-physical nonlinear circuit model with device/physical parameters for HEMTs," *International Journal of Microwave and Wireless Technologies*, vol. 3, no. 1, pp. 25–33, February, 2011.
- [e] M. Thorsell, K. Andersson, H. Hjelmgren, and N. Rorsman "Characterization of Electro-Thermal Effects in GaN Based HEMTs," in *5th Space Agency - MOD Round Table Workshop on GaN Component Technologies*, Noordwijk, Netherlands, September, 2010.
- [f] I. Angelov, M. Thorsell, K. Andersson, A. Inoue, K. Yamanaka, and H. Noto "On the Large Signal Evaluation and Modeling of GaN FET," *IEICE Transactions on Electronics*, vol. E93.C, no. 8, pp. 1225–1233, August, 2010.
- [g] I. Angelov, M. Thorsell, K. Andersson, K. Yamanaka, T. Oishi, H. Otsuka, Y. Hirano, and A. Inoue "On the Compact Equivalent Circuit Modeling of GaN FET," in *Invited Workshop, Asia-Pacific Microwave Conference*, Yokohama, Japan, December, 2010.
- [h] M. Thorsell, and K. Andersson "Active Harmonic Load-Pull using LSNA," in *2009 RF Measurement Technology for State of the Art Production and Design*, Gävle, Sweden, October, 2009.
- [i] P. Saad, H.M. Nemati, M. Thorsell, K. Andersson, C. Fager "An Inverse Class-F GaN HEMT Power Amplifier with 78 % PAE at 3.5 GHz," in *39th European Microwave Conference*, Rome, Italy, October, 2009.
- [j] H.M. Nemati, C. Fager, M. Thorsell, and H. Zirath "High-Efficiency LDMOS Power-Amplifier Design at 1 GHz Using an Optimized Transistor Model," *IEEE Transactions on Microwave Theory and Techniques*, vol. 57, no. 7, pp. 1647–1654, July, 2009.

- 
- [k] M. Thorsell, K. Andersson, M. Fagerlind, M. Södow, P.-Å. Nilsson, and N. Rorsman "Thermal characterization of the intrinsic noise parameters for AlGa<sub>N</sub>/Ga<sub>N</sub> HEMTs," in *2008 IEEE MTT-S International Microwave Symposium Digest*, Atlanta, GA, USA, June, 2008.
- [l] M. Thorsell, K. Andersson, M. Fagerlind, M. Södow, P.-Å. Nilsson, and N. Rorsman "Characterization of the temperature dependent access resistances in AlGa<sub>N</sub>/Ga<sub>N</sub> HEMTs," in *2008 Workshop on Integrated Nonlinear Microwave and Millimetre-Wave Circuits*, Malaga, Spain, November, 2008.
- [m] M. Södow, M. Fagerlind, M. Thorsell, K. Andersson, N. Billström, P.-Å. Nilsson, and N. Rorsman "An AlGa<sub>N</sub>/Ga<sub>N</sub> HEMT-Based Microstrip MMIC Process for Advanced Transceiver Design," *IEEE Transactions on Microwave Theory and Techniques*, vol. 56, no. 8, pp. 1827–1833, August, 2008.
- [n] M. Södow, H.M. Nemati, M. Thorsell, U. Gustavsson, K. Andersson, C. Fager, P.-Å. Nilsson, J. Hassan, A. Henry, E. Janzen, R. Jos, and N. Rorsman "SiC Varactors for Dynamic Load Modulation of High Power Amplifiers," *IEEE Electron Device Letter*, vol. 29, no. 7, pp. 728–730, July, 2008.
- [o] M. Södow, K. Andersson, M. Fagerlind, M. Thorsell, P.-Å. Nilsson, and N. Rorsman "A Single-Ended Resistive X-Band AlGa<sub>N</sub>/Ga<sub>N</sub> HEMT MMIC Mixer," *IEEE Transactions on Microwave Theory and Techniques*, vol. 56, no. 10, pp. 2201–2206, October, 2008.



# Notations and abbreviations

## Notations

$\Gamma_L$	Load reflection coefficient
$\Gamma_{opt}$	Optimum source reflection coefficient
$\Gamma_S$	Source reflection coefficient
$\mu_e$	Electron mobility
$\omega$	Angular frequency
$E_a$	Activation energy
$F_{min}$	Minimum noise figure
$F_n$	Noise figure
$k_B$	Boltzmann's constant
$n_s$	Electron density
$q$	Electron charge
$r_c$	Contact resistivity
$R_d$	Drain resistance
$R_g$	Gate resistance
$R_{HF}$	High electric field resistance
$R_{LF}$	Low electric field resistance
$R_N$	Noise resistance
$R_s$	Source resistance
$R_{series}$	Series resistance
$r_{sheet}$	Sheet resistivity
$T_A$	Ambient temperature
$T_{CH}$	Channel temperature
$v_e$	Electron velocity
$W_e$	Stored electric energy
$W_m$	Stored magnetic energy
$Z_C$	Characteristic impedance
$Z_L$	Load impedance
$Z_{TH}$	Thermal impedance

## Abbreviations

2DEG	Two Dimensional Electron Gas
AESA	Active Electronically Scanned Array
AlGaN	Aluminium-Gallium-Nitride
AWG	Arbitrary Waveform Generator
BCB	Benzocyclobutene
BLA	Best Linear Approximation
CW	Continuous Wave
DC	Direct Current
DLM	Dynamic Load Modulation
DUT	Device Under Test
GaAs	Gallium-Arsenide
GaN	Gallium-Nitride
GSG	Ground Signal Ground
HEMT	High Electron Mobility Transistor
HPA	High Power Amplifier
LDMOS	Laterally Diffused Metal Oxide Semiconductor
LNA	Low Noise Amplifier
LO	Local Oscillator
LSNA	Large Signal Network Analyser
MMIC	Monolithic Microwave Integrated Circuit
MTTF	Mean Time To Failure
PA	Power Amplifier
RF	Radio Frequency
SiC	Silicon-Carbide
SPDT	Single Pole Double Throw
TLM	Transfer Length Method
VNA	Vector Network Analyser
VSG	Vector Signal Generator

# Contents

<b>Abstract</b>	<b>iii</b>
<b>List of Publications</b>	<b>v</b>
<b>Notations and abbreviations</b>	<b>ix</b>
<b>1 Introduction</b>	<b>1</b>
<b>2 Electrothermal characterisation and modeling</b>	<b>5</b>
2.1 Electron transport in AlGa <sub>N</sub> /Ga <sub>N</sub> 2DEG . . . . .	6
2.1.1 TLM test structure . . . . .	8
2.1.2 Sheet resistivity . . . . .	8
2.1.3 Thermal impedance . . . . .	10
2.1.4 Isothermal IV . . . . .	12
2.1.5 Channel temperature . . . . .	14
2.2 Electrothermal model . . . . .	14
2.2.1 Thermal impedance . . . . .	15
2.2.2 Current transport . . . . .	15
2.2.3 Model verification . . . . .	17
2.3 Ga <sub>N</sub> for low noise applications . . . . .	17
2.3.1 Temperature dependent noise characterisation . . . . .	18
2.4 Monolithic transceiver front-end . . . . .	20
2.4.1 Receiver front-end . . . . .	22
2.4.2 Transceiver front-end . . . . .	24
<b>3 Nonlinear characterisation</b>	<b>27</b>
3.1 Active load-pull . . . . .	28
3.1.1 Measurement setup . . . . .	30
3.1.2 Optimisation routine . . . . .	31
3.1.3 Measurement results . . . . .	32
3.2 Dynamic load modulation . . . . .	34
3.3 Nonlinear characterisation of SiC varactors . . . . .	37
3.4 Linear approximation . . . . .	39
3.4.1 Extending the BLA . . . . .	41
3.4.2 Extended BLA measurements . . . . .	41
<b>4 Summary of appended papers</b>	<b>45</b>

<b>5 Conclusions</b>	<b>47</b>
5.1 Future work . . . . .	48
<b>Acknowledgments</b>	<b>49</b>
<b>Bibliography</b>	<b>51</b>
<b>Appended Papers</b>	<b>61</b>

# Chapter 1

## Introduction

The 19th century mathematical physicist Lord Kelvin said that *"To measure is to know."* and *"If you can not measure it, you can not improve it."* These quotations are still very true, especially for emerging semiconductor materials such as aluminium gallium nitride / gallium nitride (AlGaN/GaN). Furthermore, measurements are the basis for highly accurate models, needed for circuit design or linearisation of high efficiency amplifiers. Measurements are also very important as feedback to the device manufactures on how processing parameters affect the microwave performance of their devices. For example, how to scale the device to obtain the optimum performance for a specific task, or how different surface passivations on AlGaN/GaN affects the low frequency dispersion.

The time from the first working AlGaN/GaN high electron mobility transistor (HEMT) to commercialisation is relatively short. The first observation that the AlGaN/GaN heterostructure forms a two dimensional electron gas (2DEG) was reported in 1992 [1], and the AlGaN/GaN HEMT followed the next year by the same research group [2]. The material properties AlGaN/GaN heterostructure are very promising with an electron mobility in the range of  $2000 \text{ cm}^2/\text{Vs}$ , and an electric breakdown field of  $3.3 \text{ MV/cm}$  [3]. The AlGaN/GaN HEMT is expected to provide both high frequency operation, and high output power density. The first RF performance was reported in 1994, showing  $f_T$  and  $f_{max}$  figures of 11 and 35 GHz respectively [4]. The RF output power was later characterised in 1996, with a measured power density of  $1.1 \text{ W/mm}$  and a power added efficiency of 18% [5]. These figures have steadily improved since these first reports, with  $f_T$  and  $f_{max}$  figures of 260 and 394 GHz respectively today [6], and a power density of up to  $40 \text{ W/mm}$  [7]. The rapid increase in device performance from the first measurements to the state-of-the-art performance today is shown in Fig. 1.1.

The astonishing development in performance makes GaN based HEMTs interesting in many different areas, and has attracted a lot of interest both from universities as well as world leading semiconductor device manufacturers.

The commercialisation started in 2005 by Eudyna Devices Inc. (now Sumitomo Electric Industries, Ltd.) with the release of a discrete 10 W GaN HEMT. The output power from commercial discrete GaN based HEMTs is today at least 240 W, and commercial GaN MMIC processes are available with HEMTs

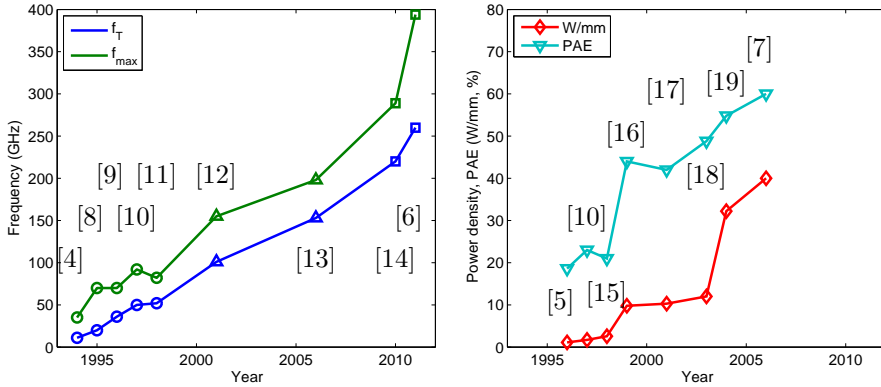


**Figure 1.1:** Development of the highest reported performance figures for GaN based HEMTs. Left:  $f_T$  and  $f_{max}$  development, markers corresponds to approximate nominal gate lengths as follows, circles 250 nm, triangle 100 nm, square 45 nm. Right: Power density and corresponding efficiency.

having power densities in the order of 5 W/mm [20, 21]. Simultaneously, the research community is still trying to understand the fundamental properties of the AlGaIn/GaN heterostructure. The high output power in combination with high frequency operation (1.7 W at 91 GHz [22]) introduce new problems in device characterisation. The very high power density, up to twenty times higher than GaAs pHEMT (1.6 W/mm [23]), put demands on the thermal conductivity of the semiconductor material, and the mounting of the transistor. The power is dissipated in a small surface area, and could cause significant self-heating. The increase in temperature affects physical parameters such as electron mobility and electron saturation velocity, and could significantly influence the performance of the transistor. Furthermore, self-heating is a dynamic process, and hence a modulated stimuli could cause the operating temperature to vary during the excitation. The dynamically varying operating temperature could therefore cause memory effects, and hence influence performance and linearity of an amplifier. It is therefore important to characterise these effects, and extend the models to correctly handle self-heating by using an accurate thermal impedance model. The large self-heating is illustrated in Fig. 1.2 with an infrared image of a packaged 9.6 mm wide GaN based HEMT dissipating 3 W of DC power. The intrinsic temperature is increased by at least 15 °C.

Since the 1950s, microwave devices are usually characterised by using a vector network analyser (VNA) [24]. The VNA provides the frequency response of the microwave network under test, i.e. the reflection and transmission of the system (the S-parameters [25]). Measurements can be carried out on both passive and active devices. However, measurements are limited to devices operating in a linear regime. It is often an assumption that the device under test (DUT) is linear, but in most cases this is not entirely true. The transfer function of a transistor is nonlinear, and large signal excitations will generate harmonics. The DUT can also suffer from memory effects due to e.g. self-heating and trapping. The memory effects, such as a dynamically varying

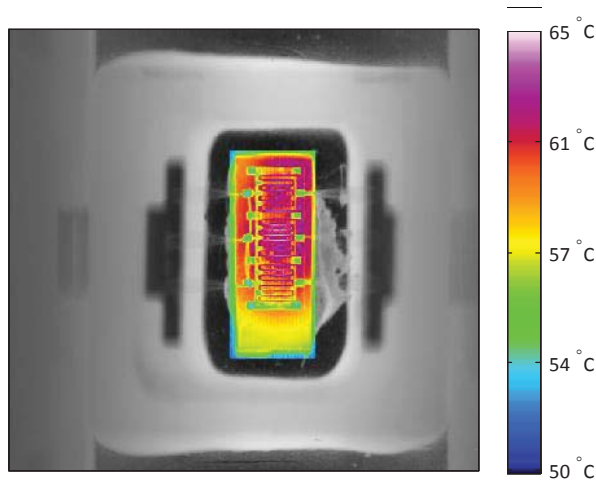


**Figure 1.2:** Infrared image of a 9.6 mm wide GaN HEMT dissipating 3 W of DC power.

temperature, will also introduce nonlinear distortion.

There is an increasing need for more accurate models, taking into account nonlinearities and memory effects, especially for telecommunication applications where high order modulation schemes are used. The increased modulation depth put high demands on the linearity of the amplifier, and linearisation techniques are needed to reduce the nonlinear distortion. Increased knowledge about the nonlinearities and memory effects in the transistor could significantly improve these models. This would allow for higher order modulation, and hence higher data rate.

It is therefore necessary to use a measurement setup that allows for the characterisation of the nonlinearities in the DUT. Such a system was first introduced in 1989 [26]. The system enables the acquisition of the magnitude and phase of the voltage and current components at the fundamental frequency and a limited number of higher order harmonics. This makes it possible to reconstruct the voltage and current waveforms at the device terminals, and gives insight into the nonlinear device operation. Furthermore, these systems allow for the acquisition of modulated signals up to a certain bandwidth [27].

Today, several commercial systems are available for nonlinear characterisation of microwave devices [28–30]. However, the main workhorses for device characterisation are still linear S-parameter measurements and scalar load-pull measurements, even for derivation of nonlinear models. The linear VNA uses the S-parameters to describe the DUT, and a similar representation is needed for the nonlinear measurement systems to simplify the transition for the users. The poly harmonic distortion (PHD) model, described in [31], is proposed as a solution to this (called X-parameters by Agilent Technologies Inc., and S-functions by NMDG NV). The PHD model can be seen as an extension to the linear S-parameters, including the relation between the different harmonics, and thus the generation of harmonics. There exists one PHD model description for each bias point, input power level, and operating frequency, hence the table based model increases in size rapidly. Furthermore, the PHD model is

load impedance dependent, and a load-pull setup is therefore required in combination with a nonlinear measurement system for a complete characterisation of a nonlinear transistor [32]. This clearly illustrates the problems with nonlinear characterisation, since the system depends on all input parameters, as well as the previous stimuli (due to memory effects), there exists no compact description of the system. It is therefore important to know the limitations of e.g. if the PHD model is valid for the used excitation or not.

This thesis tries to highlight some of the possibilities these new nonlinear measurement systems provide, and at the same time show how nonlinearities increase the uncertainty in the measurement results. The thesis is organised as follows. The electrothermal properties of the AlGa<sub>N</sub>/Ga<sub>N</sub> heterostructure are characterised in Chapter 2; in terms of electron transport, self-heating, and low noise performance. The Ga<sub>N</sub> based HEMT offers both high power and low noise, and is therefore suitable for a monolithically integrated transceiver front-end, and the first steps towards this are taken. Chapter 3 is devoted to nonlinear measurement systems. A new fast multi harmonics load-pull system is presented, and it is used for different characterisations such as knee walkout studies, dynamic load modulation, memory effect studies, and nonlinear Q-factor extraction.

## Chapter 2

# Electrothermal characterisation and modeling

The GaN based HEMT is a very promising technology, and could replace several existing semiconductor technologies in many different areas where e.g. high power, high efficiency and robustness are of interest. The material properties of the AlGa<sub>N</sub>/Ga<sub>N</sub> heterostructure indicate that very high power densities, and high frequency operation are possible. The combination of high frequency operation and high power put new demands on characterisation and modelling. The self-heating could be very large and the increased operating temperature affects material properties (e.g. electron mobility), and hence the performance of the HEMT. These effects needs to be accurately characterised and included in the models to correctly predict the response of the HEMT to any applied stimuli. An extensive electrothermal characterisation is carried out in [A], presenting new characterisation methods, and proposing a new current transport model. These results are summarised in Sections 2.1 and 2.2. The electron transport dependence on temperature and applied electric field are characterised independently using a novel isothermal method. Furthermore, the frequency response of the thermal impedance is measured by broadband impedance measurements. The thermal resistance, and thus the channel temperature are calculated by combing the different characterisation methods. These results are used to derive a new complete nonlinear electrothermal model of the access resistances in GaN based HEMTs. The thermal impedance is modelled as a distributed impedance by a  $\sqrt{j\omega}$  dependence, in contrast to the commonly used lumped RC-networks ( $j\omega$  dependence) [33]. Furthermore a new current versus electric field model is proposed, taking into account the nonlinear sheet resistivity.

The GaN based HEMT also shows promising low noise performance. Low noise operation in combination with high breakdown voltage could enable very robust GaN based receivers. The possibility to manufacture high power amplifiers and low noise amplifiers on the same die enables monolithically integrated transceiver front-ends for high power operation. Therefore, the low noise char-

acteristics needs to be measured and modelled, which is carried out in [B]. The characterisation is performed versus temperature to include both self-heating and operation at elevated temperatures. The results are summarised in Section 2.3. The first step towards a GaN based integrated transceiver front-end is taken in [C], where a receiver front-end is shown. The receiver and a first attempt on a GaN based monolithically integrated transceiver front-end are presented in Section 2.4.

## 2.1 Electron transport in AlGaIn/GaN 2DEG

The electron transport through the AlGaIn/GaN two dimensional electron gas (2DEG) determines the performance of the transistor in terms of  $f_T$ , output power and efficiency. It is therefore important to understand how the electron transport is affected by both temperature and high electric fields since the GaN based HEMT is usually operated at high voltages and high output powers. The access resistances are set by the properties of the AlGaIn/GaN 2DEG, and these directly affect the performance of the HEMT. The efficiency is decreased by increasing on-resistance, and the output power is limited by the maximum current. There have been several studies on how the access resistances affect the performance, and what parameters affect the resistance values, such as bias and temperature.

It was observed in [34] that the electron velocity exhibited an earlier saturation than expected from Monte Carlo simulations, and that the access resistances depends on the drain current. The bias dependent access resistances limited the high frequency performance, due to significantly lower extrinsic  $f_T$ . The study in [35] concludes that the access resistances are nonlinear, due to space-charge limited current conditions. A significant impact on the large signal performance is observed in terms of both output power and linearity. The bias dependence was also studied in [36], showing the impact on the intrinsic small signal parameters. The study in [37] observed a small bias dependence of the access resistances, but did not observe a decreased linearity due to dynamic access resistances.

The papers reporting bias dependent access resistances have all performed measurements on complete HEMT structures. A direct extraction method is therefore needed to determine the values of  $R_s$  and  $R_d$ . The ColdFET method [38] gives only the unbiased value of the access resistances, and a HotFET method is needed to extract the bias dependences. However,  $g_m$  and  $R_s$  are strongly connected, and not easily separated. The connection between extrinsic and intrinsic  $g_m$  includes  $R_s$ , according to:

$$g_m = \frac{g_{m,ext}}{1 - g_{m,ext}R_s}. \quad (2.1)$$

Therefore, any error in the extraction of the bias dependence in  $g_m$ , results in a bias dependence in  $R_s$ . It is therefore difficult to accurately extract the bias dependence. Furthermore, the extractions in [34–37] do not include the effects of self-heating and temperature dependence in the material properties.

The access resistances are determined by the electron mobility ( $\mu_e$ ), electron velocity ( $v_e$ ) and electron density ( $n_s$ ) of the semiconductor material. It has been shown that both  $v_e$  and  $n_s$  show a weak dependence on temperature,

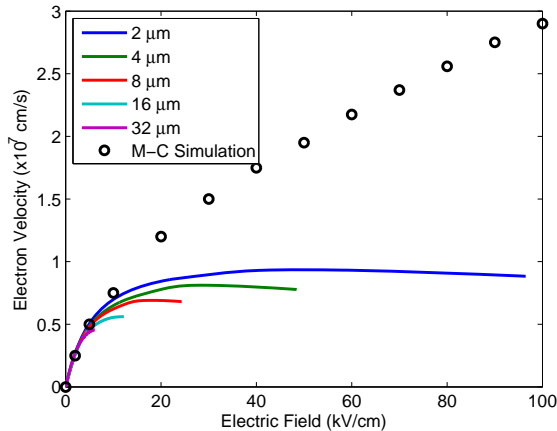


**Figure 2.1:** The measured electron velocity versus applied electric field of the  $2 \times 100 \mu\text{m}$  co-planar TLM test structure with contact separations from  $2 \mu\text{m}$  up to  $32 \mu\text{m}$ . Simulation data from Monte Carlo simulation in [43].

while the electron mobility shows a very strong dependence [39–41]. The temperature dependence in  $\mu_e$  affects the access resistances ( $R_s$  and  $R_d$ ), and a strong dependence in these have been verified in [A, B]. Furthermore, the impact of the access resistances on the high frequency performance was studied in [42], indicating significantly improved performance of GaN based HEMTs in terms of increasing  $f_T$  at low temperatures.

Monte Carlo simulation of the current transport through the AlGaIn/GaN 2DEG show that the current is expected to increase up to an electric field of at least  $120 \text{ kV/cm}$  [43]. However, this is not in line with IV measurements on the AlGaIn/GaN 2DEG, shown in Fig. 2.1. The current saturates at much lower electric fields than expected, and it was in [44] concluded that the saturation is mainly due to self-heating.

The GaN based HEMT suffer from significant self-heating, and channel temperatures of several hundred degree Celsius have been measured [45]. The self-heating combined with the strong temperature dependence in the electron mobility could have a large effect on the performance of the GaN based HEMTs. It is therefore important to accurately characterise the temperature dependence and its influence on both the power and noise performance.

Due to the strong correlation between bias dependence and temperature dependence, it is hard to isolate these two effects. It is therefore necessary to use a characterisation method where the bias and temperature dependence are isolated to obtain an accurate nonlinear model of the access resistances. The thermal response of in the AlGaIn/GaN heterostructure is very fast, and according to simulations in [46], pulse lengths of a few ns are needed for isothermal measurements.

A new characterisation method is therefore proposed in [A], separating the bias and temperature dependence. The method make use of a new test structure, described in Section 2.1.1. The temperature dependence of the

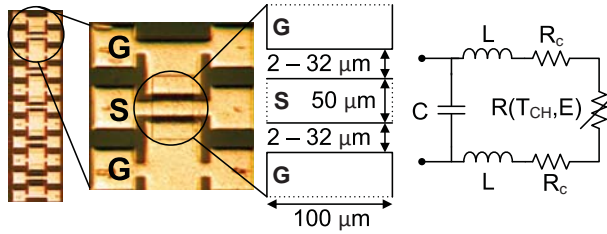


**Figure 2.2:** The 2x100  $\mu\text{m}$  co-planar TLM test structure with contact separations ranging from 2  $\mu\text{m}$  to 32  $\mu\text{m}$ .

sheet resistivity is measured in Section 2.1.2 without influence of self-heating. The frequency response of the thermal impedance is characterised by broadband frequency response measurements in Section 2.1.3. The current transport through the AlGaIn/GaN 2DEG is measured isothermally using a nonlinear measurement system in Section 2.1.4. The results from these characterisation methods are combined to enable the calculation of the channel temperature in Section 2.1.5.

### 2.1.1 TLM test structure

The transfer length method (TLM) is commonly used to characterise contact resistivity ( $r_c$ ) and sheet resistivity ( $r_{sheet}$ ) in semiconductor materials [47]. The material properties are extracted using the following model:

$$R_{meas} = 2\frac{r_c}{W} + r_{sheet}\frac{L}{W}, \quad (2.2)$$

where  $R_{meas}$  is the measured resistance,  $W$  the contact width, and  $L$  the contact separation.

The sheet resistivity is a measure of the electron mobility and electron density ( $1/r_{sheet} = qn_s\mu_e$ ), and for a GaN based HEMT,  $r_{sheet}$  equals the resistivity of the 2DEG. The TLM structure can therefore be used to characterise the access resistances of the complete HEMT. The standard TLM layout is designed with needle probes in mind, where quick measurements during processing are the aim. The needle probes work very well for IV measurements, but limits the possibilities for pulsed and RF measurements.

A new TLM structure is therefore developed, targeted for the process in [m], to allow for both DC and RF measurements. The new test structure allows for RF measurements due to use of ground-signal-ground (GSG) probe pads, as shown in Fig. 2.2. The structures layout is similar to a two finger HEMT, without the gate. It can therefore directly be used to model the access resistances of a GaN based HEMT. The total width of the contacts is 200  $\mu\text{m}$ , and the separation between the contacts is varied from 2  $\mu\text{m}$  up to 32  $\mu\text{m}$ .

### 2.1.2 Sheet resistivity

The temperature dependence of the sheet resistivity  $r_{sheet}$  and contact resistivity  $r_c$  are characterised at low electric fields. The low electric fields minimise

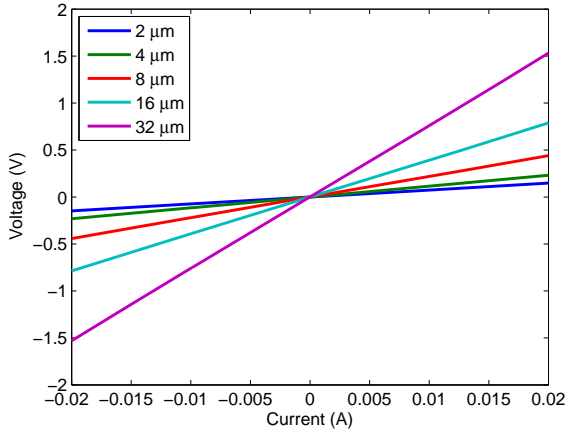


**Figure 2.3:** Resistance measurement at room temperature for the contact separations between 2  $\mu\text{m}$  and 32  $\mu\text{m}$ .

the power dissipation, and hence reduces the effects of self-heating. The channel temperature ( $T_{CH}$ ) during the TLM characterisation is therefore assumed to be equal to the ambient temperature. The ambient temperature is set by using a temperature controlled chuck.

The resistance of each contact separation is characterised by sweeping the current from -20 mA to 20 mA, and measuring the corresponding voltage over the test structure. The resistance is then obtained from the slope of a linear fit of the measured data. This method reduces systematic measurement errors, such as offsets in the voltage or current readings. Furthermore, the influence of self-heating can be estimated by determining the linearity of the measured data. The self-heating can be assumed to be insignificant if a good linear fit is obtained. The measured results of the contact separations between 2  $\mu\text{m}$  and 32  $\mu\text{m}$  are shown in Fig. 2.3, and excellent linear fits are obtained. This verifies the assumption that self-heating is insignificant, and the channel temperature equals the ambient temperature.

The TLM characterisation is carried out from room temperature up to 170  $^{\circ}\text{C}$ , and the measurements are shown in Fig. 2.4. The extracted contact resistivity is shown to be constant versus temperature (intersection point with the Y-axis in Fig. 2.4), while the sheet resistivity, corresponding to the slope, shows strong temperature dependence. The temperature dependence in  $r_{sheet}$  is mostly due to the temperature dependence in  $\mu_e$ , and can be modelled according to:

$$r_{sheet}(T_{CH}) = r_0 \left( \frac{T_{CH}}{T_n} \right)^{r_1}, \quad (2.3)$$

where  $r_0$  and  $r_1$  are fitting parameters, and  $T_n$  is a normalisation temperature.

It is clear from the TLM characterisation that the electron transport is indeed a strong function of temperature. It is therefore necessary to accurately know the temperature of the DUT during the characterisation to correctly extract the access resistances  $R_s$  and  $R_d$ .

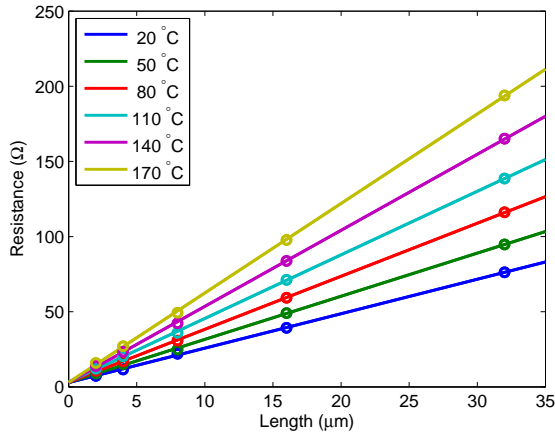


**Figure 2.4:** TLM characterisation versus temperature.

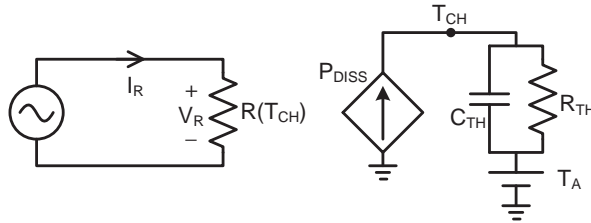


**Figure 2.5:** Illustration of the thermal impedance model.

### 2.1.3 Thermal impedance

The channel temperature ( $T_{CH}$ ) can, due to self-heating, be significantly higher than the ambient temperature ( $T_A$ ). This is due to the dissipated power ( $P_{diss}$ ) within the transistor and the thermal transport set by the thermal impedance ( $Z_{TH}$ ), according to the definition of the channel temperature:

$$T_{CH} = Z_{TH}(\omega)P_{diss}(\omega) + T_A. \quad (2.4)$$

The thermal impedance is set by the thermal conductivity and thermal capacity of the semiconductor material and the mounting of the die, and is usually modelled by a low-pass RC-network. The influence on  $T_{CH}$  due to different excitation frequencies is illustrated with a simulation of a resistor with a thermal network connected to it, according to Fig. 2.5. The resistor is  $20 \Omega$ , and the thermal network, corresponding to the thermal impedance, has a thermal resistance ( $R_{TH}$ ) of  $20 \text{ K/W}$ , and a thermal capacitance ( $C_{TH}$ ) of  $200 \text{ J/K}$ . The ambient temperature is set by a voltage source to  $25 \text{ }^\circ\text{C}$ , and the dissipated power ( $P_{DISS} = V_R I_R$ ) is treated as a current source.

A sinusoidal excitation with an amplitude of  $10 \text{ V}$  is applied over the resistor, and the frequency is swept from  $1 \text{ Hz}$  up to  $1 \text{ GHz}$ . The corresponding  $T_{CH}$  for different frequencies are shown in Fig. 2.6, and it shows that the temperature varies dynamically at lower excitation frequencies. It is also shown

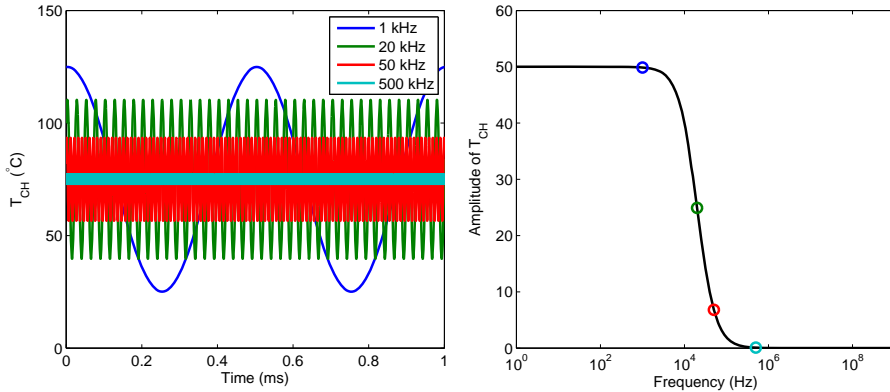


**Figure 2.6:** Self-heating simulation of a resistor. Left: Dynamically varying  $T_{CH}$  versus excitation frequency. Right: Frequency response of the amplitude of  $T_{CH}$ . Markers correspond to simulations in the left figure.

that the temperature is roughly constant for high frequency excitations, but significantly higher than  $T_A$ . This is due to that the average dissipated power excites the thermal impedance at DC. The temperature is therefore set by  $R_{TH}$  and the average dissipated power. The amplitude of the dynamically varying  $T_{CH}$  versus excitation frequency clearly show the response due to the low pass RC-network, and the dynamic self-heating is for this simulation kept to a minimum by using an excitation above 1 MHz.

The simulation illustrates the importance of correctly modelling the frequency response of the thermal impedance. This is especially true for devices which suffer from memory effects due to self-heating. An incorrect frequency response in the thermal impedance could significantly influence modulated simulations where the envelope of the signal could vary the temperature dynamically.

The most common method to reduce self-heating is by pulsed measurements, with pulse length sufficiently short to not trigger the thermal response, and with low enough duty cycle to reduce the average dissipated power. Pulsed measurement can therefore be used to characterise the bias dependence in the access resistances, to verify the studies in [34–36]. However, the needed pulse length, where the thermal response becomes insignificant needs to be known to be able to reduce the self-heating effects. Pulsed measurements on the AlGaIn/GaN 2DEG have indicated that pulses as short as 3 ns are needed for isothermal measurements [48]. The thermal response depends on both the mounting of the die, and the epitaxial layers. Hence, it is necessary to characterise the response on the used sample.

According to [49], the time constants in the thermal response are related to the time constants of the input impedance. The relationship is given by:

$$Z_{in}(\omega) = \frac{1 - \frac{\partial I(V,T)}{\partial T} Z_{TH}(\omega) V_Q}{\frac{\partial I(V,T)}{\partial V} - \frac{\partial I(V,T)}{\partial T} Z_{TH}(\omega) I_Q}, \quad (2.5)$$

where  $V_Q$  and  $I_Q$  gives the operating bias point and  $I(V, T)$  is the voltage and

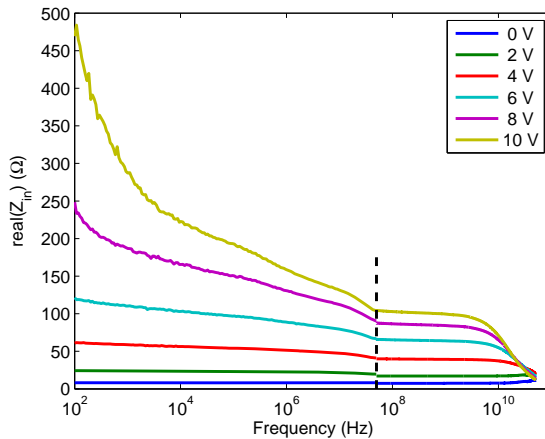


**Figure 2.7:** The input impedance at different bias voltages versus frequency. The dashed line indicates the change between two measurement regions, each measured using different setups.

temperature dependent current.

The frequency response of the thermal impedance can therefore be obtained by broadband frequency response measurements of the input impedance of the DUT. The TLM test structure allows for RF measurements, and the measured intrinsic input impedance is shown in Fig. 2.7.

The measurements of the input impedance show a response up to at least 10 MHz, and maybe up to 100 MHz. This implies that sub 10 ns pulses are needed to remove the effects of self-heating, which is in line with measurements and simulations in [46, 48]. The response around 3 GHz is due to the parasitic capacitance and inductance, seen in Fig. 2.2.

The thermal impedance needs to be known to enable characterisation without influence of self-heating. As shown in the simulation, the temperature varies dynamically when using slow excitations. Such uncertainties in the temperature, in combination with the large temperature dependence observed in the Section 2.1.2, could lead to erroneous extractions and models. It is therefore important to know the maximum frequency of the thermal response, and use an excitation well above it to enable isothermal measurements.

## 2.1.4 Isothermal IV

The need for sub 10 ns pulses to characterise the IV characteristics isothermally, as concluded in Section 2.1.3, put high demands on such a pulsed IV system. It needs to deliver a very high current during a very short time when characterising GaN based HEMTs intended for high power applications. Such measurement systems, capable of delivering high currents, are not commercially available.

A new method is therefore proposed in [A], which allows for isothermal measurements of the current versus electric field for channel widths comparable to real transistor sizes. Measurements are carried out using a Large Signal

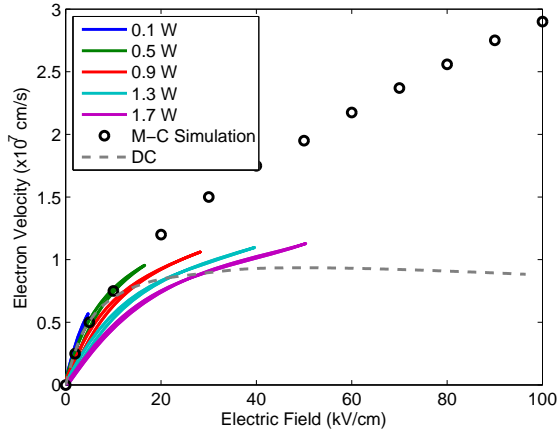


**Figure 2.8:** Intrinsic isothermal large signal measurements (lines), DC IV measurement (dashed line), and Monte Carlo simulation from [43].

Network Analyser (LSNA, MT4463 Maury/NMDG). The LSNA measures the voltage and current waveforms from 600 MHz up to 50 GHz, hence it is possible to characterise the IV characteristics of  $r_{sheet}$  in the sub ns range by measuring above 1 GHz. It is shown in Fig. 2.7 that no thermal response is present above 1 GHz, and an input signal at 6 GHz is used to be well above the thermal response of the DUT. The applied electric field is controlled by changing the input power. The increase in input power increases the average dissipated power in the DUT, causing  $T_{CH}$  to increase relative to the room temperature. However,  $T_{CH}$  is constant during the RF cycle, hence isothermal measurements at an elevated temperature are obtained, as illustrated in the simulation in Section 2.1.3. The increase in  $T_{CH}$  due to the average dissipated power could be reduce further by pulsed RF measurements, but this study uses only CW excitations. Measurement up to an electric field strength of 50 kV/cm are carried out, and the intrinsic (parasitic pad-capacitances and inductances are de-embedded) waveforms are compared to DC IV measurements and Monte Carlo simulation [43] in Fig. 2.8.

The isothermal IV-waveforms show a nonlinear current versus electric field dependence, which is in line with the Monte Carlo simulation and the pulsed IV measurements in [48]. Furthermore, the large influence of the self-heating during DC measurements is seen when comparing the isothermal waveforms with the DC measurement at room temperature (dashed line). No saturation of the current at high electric field is observed for the isothermal measurements.

The current transport through the AlGaN/GaN 2DEG is indeed bias dependent, but these studies indicates that the temperature dependence is more significant, and limits the performance of the HEMT. It is therefore necessary to measure the channel temperature to obtain an accurate electrothermal model. The model needs to take into account both the temperature, and the bias dependence of the current transport.

### 2.1.5 Channel temperature

The channel temperature is not only an important parameter for the material properties of the AlGa<sub>N</sub>/Ga<sub>N</sub> heterostructure as shown in Sections 2.1.2 - 2.1.4. The temperature also affects the reliability of the HEMT. The reliability is strongly dependent on  $T_{CH}$ , and incorrect estimations could significantly increase or decrease projected life-times. This according to the mean time to failure ( $MTTF$ ) calculation:

$$MTTF = MTTF_0 e^{\frac{-E_a}{k_B(T_0 - T_{CH})}}, \quad (2.6)$$

where  $MTTF_0$  is a measured  $MTTF$  at an elevated temperature  $T_0$ ,  $E_a$  is the activation energy, and  $k_B$  is Boltzmann's constant.

The increase in  $T_{CH}$  can be measured using direct methods such as micro Raman spectroscopy [50, 51], or infrared microscope [52]. However, the use of infrared microscopy to determine the surface temperature of Ga<sub>N</sub> based HEMTs underestimates the real temperature due to that both the SiC substrate and the Ga<sub>N</sub> layer are transparent to infrared radiation [53]. This can partly be overcome by coating the sample with black paint, but there is an increased risk in damaging the surface, and thus the transistor. The micro Raman spectroscopy method provides an accurate temperature reading with sub micron resolution, and is therefore well suited for channel temperature measurements of Ga<sub>N</sub> based HEMTs. The drawback is that it requires direct access to the surface, hence not suitable for packaged transistors.

A new method is therefore proposed in [A], by combining the measurements in Section 2.1.1 and Section 2.1.4. The differential conductivity in the low field region ( $< 3$  kV/cm) in Fig. 2.8 is increasing with dissipated power. This is due to the decrease in electron mobility with temperature, which is directly related to the increase in  $r_{sheet}$  with temperature. It is therefore possible to calculate  $T_{CH}$  by determining the differential conductivity in the low field region and use this as input in equation (2.3). The extracted low-field resistance and the corresponding  $T_{CH}$  are shown in Fig. 2.9.

The estimated thermal resistance for the sample is 80 K/W (16 K·mm/W), which is in line with micro Raman spectroscopy measurements [44, 45, 53]. This verifies the validity and high accuracy of the proposed method to estimate  $T_{CH}$ .

The knowledge of  $T_{CH}$  enable the extraction of accurate electrothermal models, taking into account both the temperature and bias dependence of the current transport through the AlGa<sub>N</sub>/Ga<sub>N</sub> 2DEG. Such models, including a correct value for  $T_{CH}$  can directly predict parameters such as nonlinear distortion due to the nonlinear access resistances. Furthermore, the reliability is affected by the operating temperature. This is important to take into account when using the Ga<sub>N</sub> HEMT in commercial products.

## 2.2 Electrothermal model

A complete electrothermal model of the access resistances is derived and verified in [A]. It is based on the characterisation in Section 2.1, and includes the effects of both self-heating and electric field dependence. The new characterisation method allows for the separation between self-heating and bias

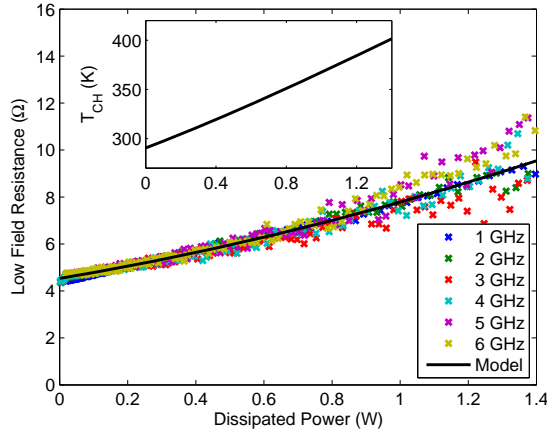


**Figure 2.9:** The low field resistance versus dissipated power and the corresponding  $T_{CH}$  according to (2.3) in the inset.

dependence, which needs to be included in the model. This results in the need for new models to correctly and accurately take these effects into account.

### 2.2.1 Thermal impedance

The thermal impedance is usually modelled with lumped RC networks to obtain a low-pass frequency response. However, the time constants seen for the measurements in Fig. 2.7 show a slower decay than expected from an RC time constant. The thermal impedance is, according to [33], distributed and should be modelled by a  $\sqrt{j\omega}$  dependence. It is also observed that multiple time constants are present in Fig. 2.7, and hence the thermal impedance of the TLM test structure is given by the sum of these according to:

$$Z_{TH}(\omega) = \sum_{k=1}^n \frac{R_{THk}}{1 + \sqrt{j\omega R_{THk} C_{THk}}}, \quad (2.7)$$

where  $R_{THk}$  is the thermal resistance, and  $C_{THk}$  is the thermal capacitance. Two time constants are needed to model the response in Fig. 2.7. The total thermal resistance is given in Section 2.1.5, and is estimated to 80 K/W for the 2  $\mu\text{m}$  long test structure. The total  $R_{TH}$  needs to be divided between the two parts of the thermal impedance,  $R_{TH1}$  and  $R_{TH2}$ . The determination of  $R_{TH1}$  and  $R_{TH2}$  is carried out empirically. The resulting thermal impedance accurately predicts the frequency response of the input impedance, as shown in Fig. 2.10.

### 2.2.2 Current transport

One of the most common models to describe the nonlinear current versus electric field in semiconductors is the Caughey-Thomas model [54]. This model consists of two parts, first the low electric field region, described by the electron mobility. The second region is the saturation region, determined by the

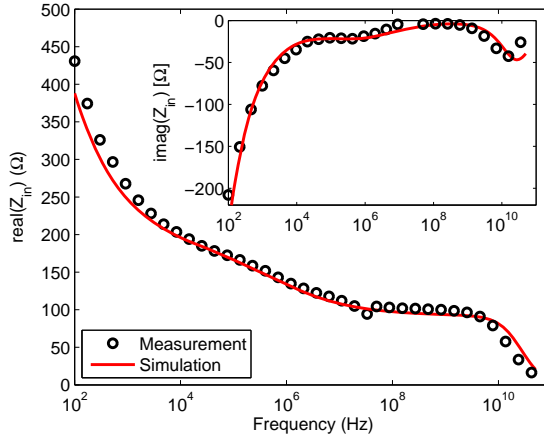


**Figure 2.10:** Measured and modeled input impedance of the  $2 \times 100 \mu\text{m}$  wide and  $2 \mu\text{m}$  long test structure.

saturation velocity of the electrons in the material. The model also includes the possibility to modify the transition between these two regions.

However, Monte Carlo simulations, and pulsed measurements indicates that the electron velocity versus electric field in the AlGaIn/GaN 2DEG follows a different behaviour [43, 48]. This is also verified by the isothermal IV measurements in Fig. 2.8. A new model is therefore proposed in [A]. The model is, similar to the Caughey-Thomas model, divided into two regions. The first region, at low electric fields, depends on the electron mobility (or low electric field resistance,  $R_{LF}$ ). The second region, in contrast to [54], does not model a saturation, but instead is modelled by a different high field mobility (or high electric field resistance,  $R_{HF}$ ). Furthermore, a temperature dependence in the two different regions is introduced, and the proposed model is given by:

$$I(E, T) = \frac{E}{R_{LF}(T)} \left( 1 + \left( \frac{|E|}{E_k(T) + \alpha(T)|E|} \right)^\beta \right)^{-1/\beta}, \quad (2.8)$$

with

$$\alpha(T) = \left( \frac{R_{HF}^\beta(T)}{R_{LF}^\beta(T)} - 1 \right)^{-1/\beta}. \quad (2.9)$$

where the temperature dependence of  $R_{LF}(T)$  is given by the sheet resistivity in (2.3). The sheet resistivity is scaled by the contact separation and contact width to get the correct  $R_{LF}(T)$  according to:

$$R_{LF}(T_{CH}) = \frac{L}{W} r_{sheet}(T_{CH}). \quad (2.10)$$

The temperature dependence of  $R_{HF}(T)$  is modelled according to:

$$R_{HF}(T) = r_{h0} \left( \frac{T}{T_n} \right)^{r_{h1}}, \quad (2.11)$$

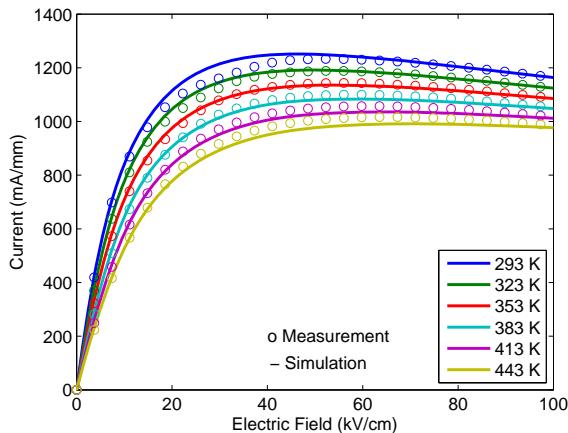


**Figure 2.11:** Measured and modeled IV characteristics of the  $2 \times 100 \mu\text{m}$  wide and  $2 \mu\text{m}$  long test structure.

where  $r_{h0}$  and  $r_{h1}$  are empirically determined fitting parameters, and  $T_n$  is a normalisation temperature.  $E_k(T)$  and  $\beta$  in (2.8) affects the transition between the two regions, and  $E_k(T)$  is modelled with a linear temperature dependence according to:

$$E_k(T) = e_0 + e_1 \frac{T - T_0}{T_n}, \quad (2.12)$$

where  $e_0$  and  $e_1$  are fitting parameters, and  $T_0$  equals 273 K.

### 2.2.3 Model verification

A complete nonlinear electrothermal model is derived for the resistance in the  $2 \mu\text{m}$  long test structure, taking into account both the self-heating and the electric field dependence. The model includes the nonlinear resistance, contact resistances and parasitic inductance and capacitances, as shown in Fig. 2.2. The IV characteristics at different ambient temperatures is shown in Fig. 2.11, and good agreement is obtained.

The model is also verified for the RF measurements in Section 2.1.4. The extrinsic waveforms (including the parasitic inductance and capacitance) are shown in Fig. 2.12, and good agreement is obtained.

## 2.3 GaN for low noise applications

The high power and high efficiency performance of the GaN based HEMT has been generally accepted for a long time [3]. The high electron mobility and high breakdown voltage making the GaN HEMT suitable for high power applications also makes the GaN HEMT interesting for use in robust receivers. Several publications report sub 1 dB noise figure at X-band [12, 55, 56], [B, m], indicating the potential of the GaN HEMT for use in LNAs. Furthermore, reports on cooled GaN based LNAs show improved performance at cryogenic

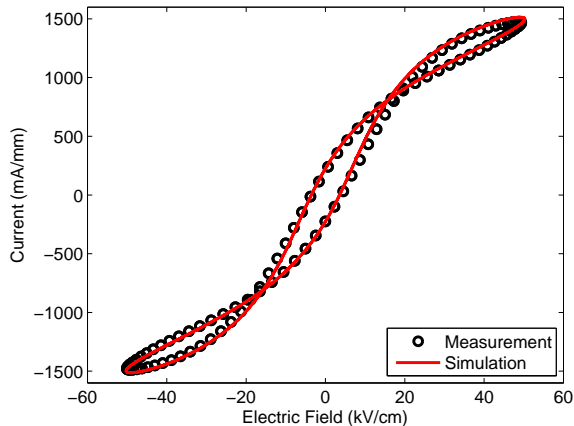


**Figure 2.12:** Measured and modelled extrinsic isothermal IV waveform at 6 GHz of the  $2 \times 100 \mu\text{m}$  wide and  $2 \mu\text{m}$  long test structure.

temperatures [57, 58]. In the following sections the noise properties are characterised and modelled as function of temperature, and the limiting factors in terms of low noise performance are identified.

### 2.3.1 Temperature dependent noise characterisation

The previous sections showed the impact of self-heating on access resistances, current transport, and performance of the GaN HEMT. This is especially important for low noise applications, where an increased operating temperature directly affects the noise properties. This is shown by calculating the rms noise voltage ( $E$ ) from a resistor ( $R$ ) kept at a certain temperature ( $T$ ) [59], according to:

$$E^2 = 4k_B T R, \quad (2.13)$$

where  $k_B$  is Boltzmann's constant. The noise voltage is linearly dependent on the temperature, and this expression is valid for any passive network by replacing  $R$  with the real part of its impedance. It should be noted that the increase in noise voltage is significantly faster than linear versus temperature for devices suffering from self-heating. The measurements in the previous sections shows that the GaN base HEMT suffer from self-heating, and the access resistances are temperature dependent. The generated thermal noise will therefore increases both due to higher temperature and due to increasing access resistances.

It can be shown that the noise figure of any two port network (both passive and active) depends on the input termination [60], and that the noise figure ( $F_n$ ) of such a two port is given by:

$$F_n = F_{min} + \frac{4R_N}{Z_C} \frac{|\Gamma_{opt} - \Gamma_S|^2}{|1 + \Gamma_{opt}|^2 (1 - |\Gamma_S|^2)}, \quad (2.14)$$

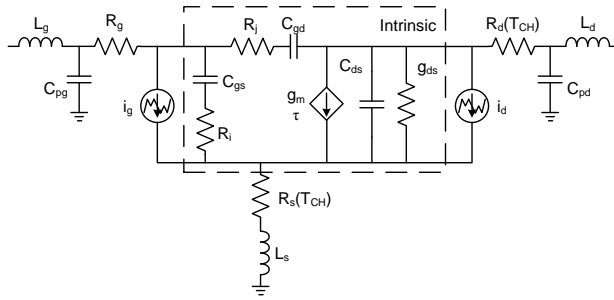


**Figure 2.13:** The small signal noise model, showing the intrinsic noise current sources.

where  $F_{min}$  is the minimum noise figure,  $R_N$  the noise resistance,  $Z_C$  the characteristic impedance, and  $\Gamma_{opt}$  the optimum source impedance. The noise parameters are measured by using an input tuner to realise different source reflection coefficients ( $\Gamma_S$ ). The noise figure of the transistor is measured for each  $\Gamma_S$ , and the noise parameters are obtained by least square fitting of equation (2.14) [61, 62].

The measured noise parameters are the extrinsic noise parameters of the transistor. The extrinsic noise includes noise from the intrinsic noise sources, as well as resistive losses in the parasitic embedding network due to the access resistances. It is necessary to extract the intrinsic noise sources to enable accurate modelling of the low noise performance. The parasitic network can be de-embedded to obtain the intrinsic noise sources by following the guidelines in [63]. The model used in this thesis is based on the PRC model in [64], and consists of one noise current source at the gate ( $i_g$ ), one noise current source at the drain ( $i_d$ ), and their correlation ( $C$ ), as shown in Fig. 2.13.

As seen in Section 2.1, the access resistances are temperature dependent, with a power dependence according to (2.10). The rms noise voltage over the access resistances is therefore according to (2.13) increasing significantly faster than linearly with temperature. The extrinsic noise parameters are measured versus temperature over the temperature range 297 - 398 K to determine the temperature dependence. The intrinsic noise parameters are obtained by de-embedding the parasitic network, taking into account the temperature dependent access resistances. The extrinsic and intrinsic noise parameters versus temperature at 9 GHz are shown in Fig. 2.14

The intrinsic minimum noise figure is roughly 0.5 dB below the extrinsic minimum noise figure. Hence, the low noise performance of the GaN HEMT is significantly limited by the source and drain access resistances ( $R_s$  and  $R_d$ ). Furthermore, the access resistances are temperature dependent as shown in Section 2.1, which explains the increasing difference between the intrinsic and extrinsic  $F_{min}$  with temperature in Fig. 2.14.

The model, described in detail in [B], includes temperature and drain current dependence of  $i_g$  and  $i_d$ . Furthermore, the model includes self-heating and temperature dependent access resistances. The agreement in the measured temperature range is good, as shown in Fig. 2.15. This clearly illustrates the importance of including thermal effects in the noise modelling of GaN based HEMTs. This conclusion is also true for Gallium Arsenide (GaAs)

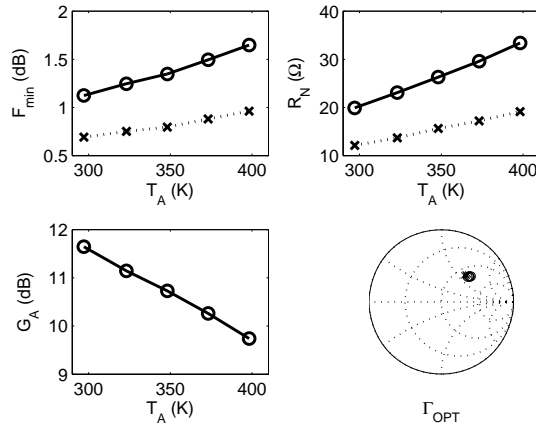


**Figure 2.14:** The extrinsic (solid) and intrinsic (dotted) noise parameters versus temperature for a  $2 \times 100 \mu\text{m}$  GaN HEMT at 9 GHz, biased at 15% of the saturated drain current.

HEMTs and other materials. The electron mobility in the GaAs 2DEG show a very large temperature dependence [65], and hence the access resistances are temperature dependent.

## 2.4 Monolithic transceiver front-end

The previous section shows that GaN based HEMTs could be an interesting candidate for use in LNAs. Several LNAs have been published, showing promising results with noise figures as low as 0.2 dB [58]. Furthermore, GaN based LNAs are very linear, with OIP3 figures of up to 54 dBm [66], and can withstand very high input powers up to 42 dBm [67]. The high breakdown voltage improves the survivability, and hence protective circuitry, such as limiters, may not be needed. The removal of the limiter could improve the overall system performance due to the relatively high losses in the limiter, typically 1.5 dB for GaAs MMIC limiters [68, 69]. The higher noise figure (typically  $< 1$  dB at 10 GHz), compared to commonly used GaAs pHEMT ( $< 0.5$  dB at 12 GHz, TriQuint MMIC process TQP13-N), could therefore be compensated by the increased robustness. These properties makes GaN based LNAs very interesting for use in radar receivers, where high survivability and low noise figure are important.

Traditionally transceiver front-ends are made up of several individual circuits, with bulky interconnects in between, as illustrated in Fig. 2.16. The circuits are typically using different semiconductor technologies with optimised manufacturing processes for either low noise or high power applications. This enables high performance, but with the cost of bulky and relatively heavy solutions.

The properties of the GaN material make both high power amplifiers (HPA) as well as robust and linear receivers possible. It is therefore an excellent candidate for radar transceiver modules, which can be accomplished by using

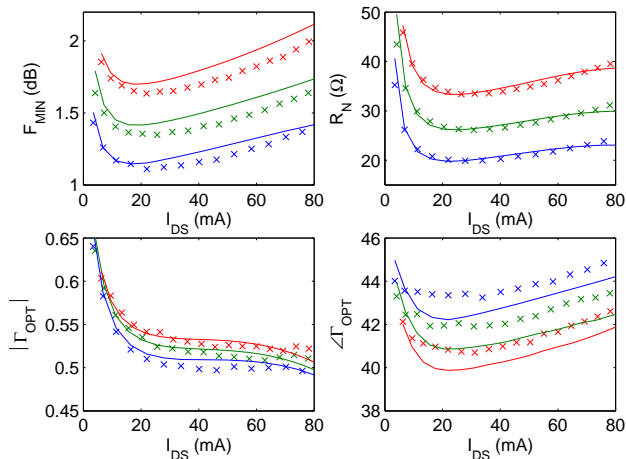


**Figure 2.15:** Modelled (line) and measured (cross) noise parameters for a  $2 \times 100 \mu\text{m}$  GaN HEMT at 9 GHz for 297 K (blue), 348 K (green) and 398 K (red).

hybrid solutions, with GaN based LNAs and HPAs as in [70]. The output power is higher than 40 dBm, and the noise figure is below 2.5 dB over the frequency band of 8 to 12 GHz. However, the transceiver front-end in [70] uses a bulky circulator at the antenna port. The circulator can be replaced with a GaN based single pole double throw (SPDT) switch, showing promising performance results with a typical insertion loss of 1 dB at X-band [71,72]. The X-band transceiver in [73] make use of only GaN based circuits in the front-end (SPDT-switch, LNA, and HPA), and obtains an output power of almost 35 dBm, and a noise figure of nearly 6 dB, the lower performance is largely due to the SPDT-switch. As suggested in [m], a GaN based transceiver could also be manufactured on one single chip in the same manufacturing process, illustrated in Fig. 2.17. This would allow for extremely small form factor and light weight solution, suitable for airborne active electronically scanned array (AESA) systems [74]. These systems use thousands of elements; hence a small form factor and light weight are required.

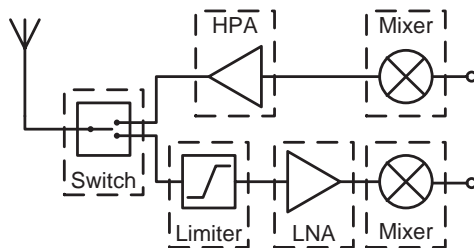


**Figure 2.16:** Schematic of a standard multi-chip transceiver front-end.

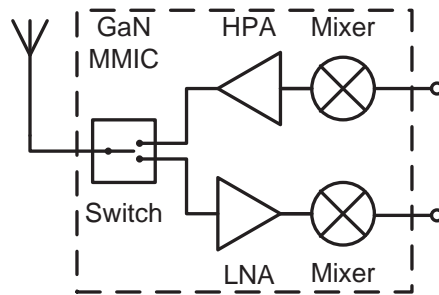


**Figure 2.17:** Schematic of a monolithically integrated GaN based transceiver front-end.

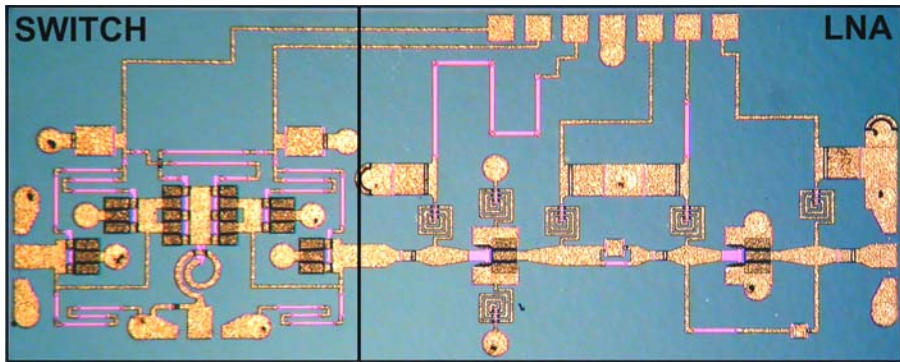


**Figure 2.18:** GaN based receiver front-end with an SPDT switch and an LNA. Chip area is 3.5 mm  $\times$  1.4 mm.

### 2.4.1 Receiver front-end

A first step towards a single chip transceiver front-end is presented in [C]. The high power capabilities of GaN based HEMTs are well known [3], but the receiver performance still needs to be evaluated. The paper presents a receiver front-end, where a SPDT switch is integrated with an LNA, shown in Fig. 2.18.

The LNA is designed for X-band operation (8-12 GHz), and the SPDT switch provides broadband operation from 2-18 GHz. The insertion loss of the broadband switch is less than 2 dB, which directly affects the noise figure of the receiver. A more narrowband switch design could be used for improving the performance of the receiver. The 0.2 dB compression point of the switch is 34 dBm, which enables high power survivability of the receiver. The operating frequency of the manufactured LNA shifted to 9-13 GHz. The frequency shift was caused by a change in the inductance values, the model included a BCB layer on top, but the fabricated inductances did not have this BCB layer. The S-parameters of the manufactured receiver front-end are shown in Fig. 2.19, where both the on- and off-states of the switch are shown. The receiver provides more than 9.6 dB of gain in the 9-13 GHz range, and the return loss is better than 8 dB.

The noise figures of both the LNA and the receiver front-end are measured

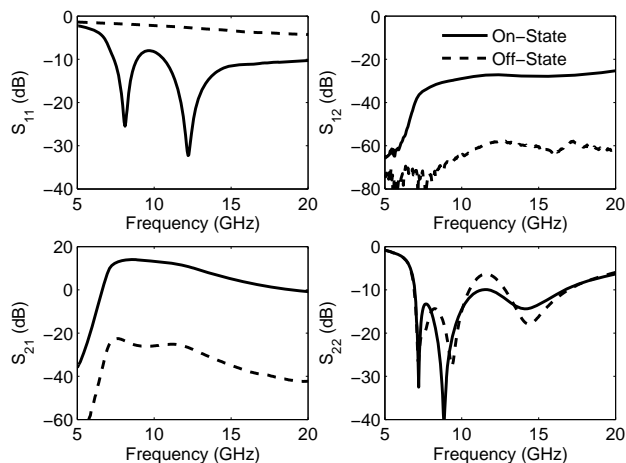


**Figure 2.19:** The S-parameters of the receiver front-end with the SPDT switch turned on and off.

and compared with the simulations. The change in the inductances is clearly visible at the lower end of the frequency band, and the characteristics are shifted by approximately 1 GHz, shown in Fig. 2.20. The noise figure of the LNA is below 2.9 dB, and the noise figure of the receiver is below 4.1 dB in the 9-13 GHz range. The switch is limiting the performance of the receiver front-end, but the size is significantly smaller compared to front-ends utilising bulky circulators or multi chip solutions [70, 73].

The benefit of reduced size and weight could very well compensate any reduction in performance. Interesting to note is that the performance of the single LNA is comparable in terms of low noise performance to GaAs based receivers with integrated limiter withstanding up to 10 W of input power [75]. The GaN based LNA is expected to survive input power levels up to at

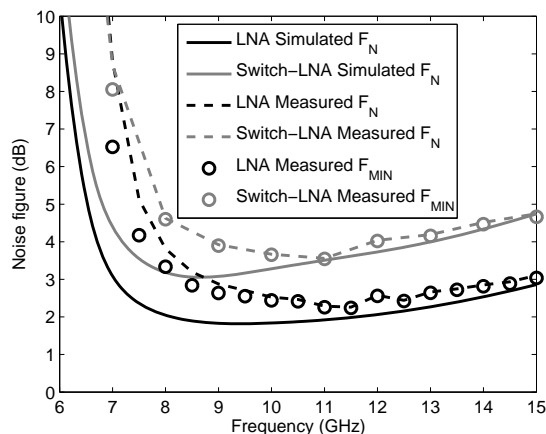


**Figure 2.20:** Noise figure of the receiver front-end with and without the switch at the input, compared with simulations.

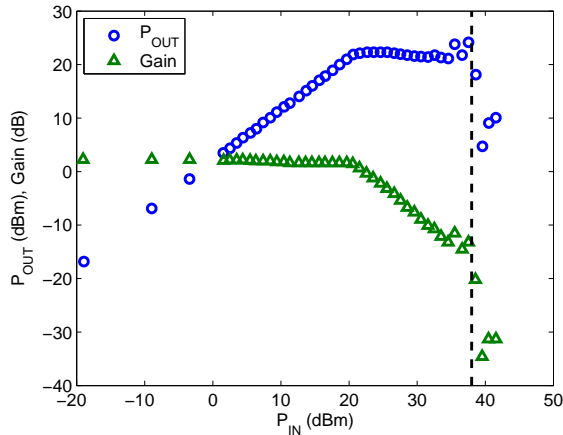


**Figure 2.21:** Survivability measurement using CW stimuli on a single stage GaN LNA operating at 7 GHz. Dashed line indicates 38 dBm of input power.

least 10 W under pulsed operation, due to the use of protective resistances in the gate bias path. Survivability measurements on a single stage GaN LNA fabricated in the same MMIC process with protective resistances showed that it withstands up to 38 dBm under CW condition (Fig. 2.21), and up to 44 dBm under pulsed condition (3  $\mu$ s pulse width and 1.5 ms pulse period).

## 2.4.2 Transceiver front-end

The next step in realising a monolithic GaN based transceiver front-end is to integrate a power amplifier with the SPDT switch and LNA in the previous section. An X-band power amplifier is designed using two  $4 \times 100$   $\mu$ m wide GaN HEMTs in a parallel configuration, as shown in Fig. 2.22.

The monolithic GaN based transceiver is manufactured using the MMIC process described in [m]. The expected performance is therefore an output power of at least 4 W (total gate width of PA is 0.8 mm), and a noise figure below 3.5 dB. The transceiver is characterised by S-parameter measurement, shown in Fig 2.23. The S-parameters indicates that the transceiver works at X-band, with a gain above 10 dB for the receiver path, and above 5 dB for the transmitter. The input and output matching are sufficient for both the receiver and transmitter paths. However, noise figure and output power measurements are still pending.

The result are promising, and manufacturing a complete monolithically GaN based transceiver front-end is feasible. This would significantly reduce the volume and weight of the RF front-end, and hence more transceiver modules could be used in an AESA system.

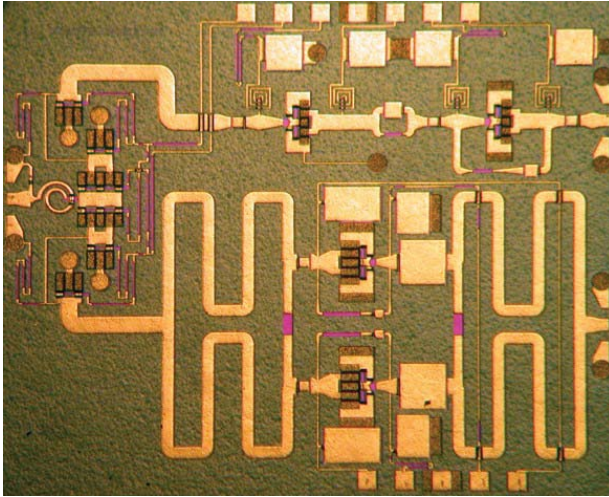


**Figure 2.22:** A monolithic GaN based X-band transceiver front-end.

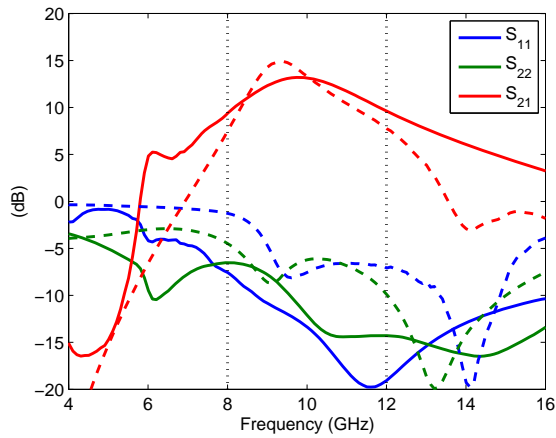


**Figure 2.23:** Measured S-parameters of the X-band transceiver front-end. Solid lines are the receiver path, and dashed lines are the transmitter path.



## Chapter 3

# Nonlinear characterisation

The standard procedure used for many years when characterising transistors is to perform DC measurements to get the IV characteristics, and use a VNA to obtain the S-parameters at each operating bias point. These measurements are either performed under CW condition, or under pulsed condition to reduce the thermal effects. These characterisation methods work very well as long as the transistors behave linearly. For a linear operating device, the S-parameters will correctly predict the response to any applied stimuli (if stimuli is small with respect to the operating point values). However, the response due to a large signal excitation is not characterised. Hence effects such as harmonic generation, gain compression, and intermodulation distortion are not included. The nonlinearities in the device are classified as odd and even, where the odd order nonlinearities causes in-band distortion, and the even order nonlinearities generate a low frequency response around DC. The response at DC, due to a large signal excitation, could give information about memory effects such as self-heating and trapping. These effects can significantly affect device performance, and are not visible in IV and S-parameter measurements.

It is necessary to characterise the DUT under large signal excitation to get information about the nonlinear distortion. The VNA is therefore no longer a suitable instrument, and a replacement is needed. The magnitude and phase of the generated harmonics due to the nonlinearity of the device needs to be measured to obtain a complete characterisation of the device operation. Due to practical limitations, only a limited number of harmonics can be measured, and hence sufficiently many needs to be included. Such a measurement system, capable of measuring the magnitude and phase of the harmonics is presented in [26]. The system is limited to CW measurements, and utilise a mixer based approach to measure the RF spectrum. A sampling based measurement system is introduced in [76], enabling the simultaneous measurement of multiple harmonics. The sampler based instrument is extended in [27] to enable modulated and pulsed measurements by measuring a limited bandwidth around each harmonic. The mixer based approach is further developed in [77] to allow for modulated measurements. There are advantages and disadvantages with the sampler and mixer based measurement systems, and the two systems are compared in [78]. The conclusion is that none of the two methods can be said to be superior to the other. All nonlinear measurements in this thesis

are carried out by using a sampler based instrument, the LSNA (MT4463, Maury Corp./NMDG NV). This allows for modulated measurements with up to 20 MHz modulation bandwidth.

The nonlinear measurement systems allow for new characterisation methods. The voltage and current waveforms of a transistor can be measured under load-pull conditions to realise different amplifier classes of operation by waveform engineering [79]. Furthermore, the waveforms allow the study of dispersion effects such as knee-walkout in GaN based HEMTs [80]. These characterisations take a significant amount of time since several different load impedance combinations need to be measured to obtain a complete characterisation. A new active load-pull setup is presented in [D], allowing for very fast load-pull measurements with waveform acquisition. The results from the setup are summarised in Section 3.1. The possibility to control the load impedance in a fast, or dynamic way, also enables new characterisation methods. Amplifier topologies such as dynamic load modulation [81] can be directly synthesised at the transistor terminals, as shown in [E], and summarised in Section 3.2.

The realisation of amplifiers for dynamic load modulation operation requires tunable components to alter the impedances, such as varactors. The varactor is a nonlinear device and will generate harmonics and intermodulation. This could affect the linearity of the amplifier, which needs to be accounted for in the design. Furthermore, the generation of harmonics acts as a loss at the fundamental frequency, and hence reduces the Q-factor of the varactor. It is therefore necessary to take the nonlinear distortion into account when characterising nonlinear devices, as shown in [G] and summarised in Section 3.3.

The output data obtained from nonlinear measurements are the voltage and current waveforms for an excitation at a single fundamental frequency, which could be a limiting factor. It is in many applications useful to obtain the frequency dependence of the nonlinear system to a large signal excitation. Linear VNA measurements sweep the excitation frequency to obtain the frequency response of the DUT. However, the response to a large signal excitation could, due to memory effects, differ depending on the sweep direction, measurement speed, and the chosen frequency grid. A broadband excitation, covering the frequency band of interest will due to even order nonlinearities generate a response around DC, and hence excite the memory effects. A new characterisation method to study the dynamics in low frequency dispersion is therefore presented in [F], and the results are summarised in Section 3.4.

### 3.1 Active load-pull

The commonly used S-parameters are not valid when driving the DUT with large signals, such as in power amplifiers, due to the nonlinear distortion. The output power and efficiency of a transistor depends upon input power, bias, and source and load impedances at all harmonics containing power due to the excitation signal. It is therefore necessary to characterise the performance of the transistor versus all these parameters to find the optimum combination for the desired application. The input power and bias are easily controlled, but the load and source impedances need a system capable of changing the

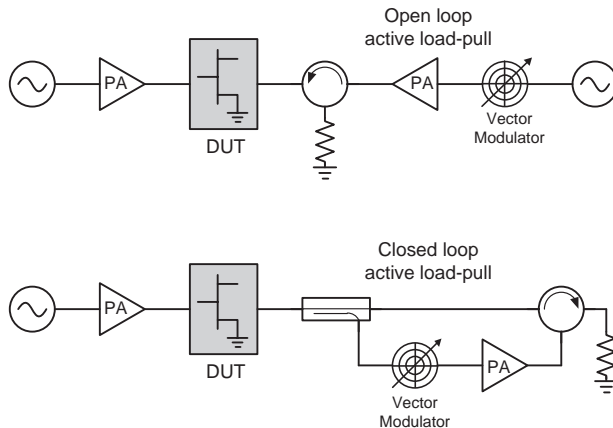


**Figure 3.1:** Comparison between open loop and closed loop active load pull setups.

reflection coefficient at the input and output of the DUT.

The classical approach to control the load impedance is to use mechanical impedance tuners [82]. The mechanical tuners are high precision mechanical instruments consisting of a slabline and at least one metal probe. The tuner is either controlled manually or automatically. Automatic tuners use stepper motors to control the distance between the slabline and the probe, and also the position of the probe along the slabline. The magnitude of the reflection coefficient presented to the device is controlled by changing the height of the probe, and the angle of reflection coefficient is set by the position of the probe along the slabline. The mechanical tuner is therefore very sensitive to mechanical disturbance, and very high repeatability in the stepper motors are needed for accurate measurements. Furthermore the speed of the mechanical tuner is limited by the speed of the stepper motors.

The load reflection coefficient ( $\Gamma_L$ ) is defined as the ratio between the outgoing voltage wave ( $b_2$ ) and the reflected (due to the load) voltage wave ( $a_2$ ), according to:

$$\Gamma_L = \frac{a_2}{b_2}. \quad (3.1)$$

Hence any load reflection coefficient may be synthesised by controlling the amplitude and phase of  $a_2$ . This can be achieved by injecting  $a_2$  rather than reflecting as done with the mechanical tuner [83]. There are two commonly used methods to control the injected signal, either the open loop approach [83], or the closed loop approach [84], illustrated in Fig. 3.1.

The closed loop active load-pull setup reuses the outgoing  $b_2$  wave, hence it achieves perfect phase coherence between the active injection and the drive signal on the input of the DUT. The load impedance is set by controlling the amplitude and phase of the decoupled signal before it is injected back towards the DUT. There is no need to measure the injected wave to determine the load impedance if the loop gain is known by a pre-calibration. The downside is that the closed loop setup suffers from significant instability problems due

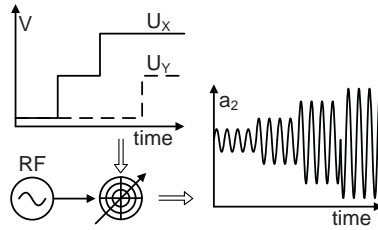


**Figure 3.2:** Illustration of the amplitude and phase control of  $a_2$  by using a vector modulator.

to potential oscillations within the closed loop.

The open loop active load-pull setup injects an additional amplitude and phase controlled signal rather than reusing the generated signal from the DUT. This removes the problems with instability related to the closed loop. The injected signal is either generated by an auxiliary signal source, or by splitting the input signal of the DUT. The phase coherence between the drive signal and the injected signal could therefore be a problem depending on the used configuration. The control of the load impedance is more difficult compared to the closed loop setup. The outgoing  $b_2$  wave needs to be measured to know how to set the amplitude and phase of the injected  $a_2$ . This requires additional measurement capabilities, and increases both the complexity of the setup and the measurement time.

The amplitude and phase of a signal can be controlled in different ways by using e.g. attenuators, phase shifters, variable gain amplifiers, I/Q mixers, vector modulators, or vector signal generators (VSGs). Depending on the setup, one or more of these are suitable. The vector modulator is used in the setup in this thesis, and a benefit compared to an I/Q mixer is the absence of LO leakage. The amplitude and phase of the vector modulator are set by two digital control signals ( $U_X$  and  $U_Y$ ), as shown in Fig. 3.2.

### 3.1.1 Measurement setup

There is an increased interest in using active injection to control the load impedances rather than using mechanical tuners. This has led to several commercial suppliers of active load-pull systems, such as Mesuro Ltd and Antevta-mw BV. The system from Mesuro is based on an oscilloscope to capture the voltage and current waveforms, and is capable of multi harmonic load-pull measurements. The measurement speed of the system is rather slow since the optimisation routine to find the impedance setting requires more than 15 iterations [85], and it does not make use of modulated measurements to increase the speed. The system from Antevta utilises modulated signals to decrease the measurement time. Multiple load impedance states or input power levels can be measured during one measurement cycle [86]. The system also enables load-pull measurements on wideband communication signals, presenting a fixed load impedance over the entire frequency band of interest [87]. However, the system is limited to load-pull measurements, and does not provide voltage or current waveforms.

None of the commercially available systems offer both fast measurements

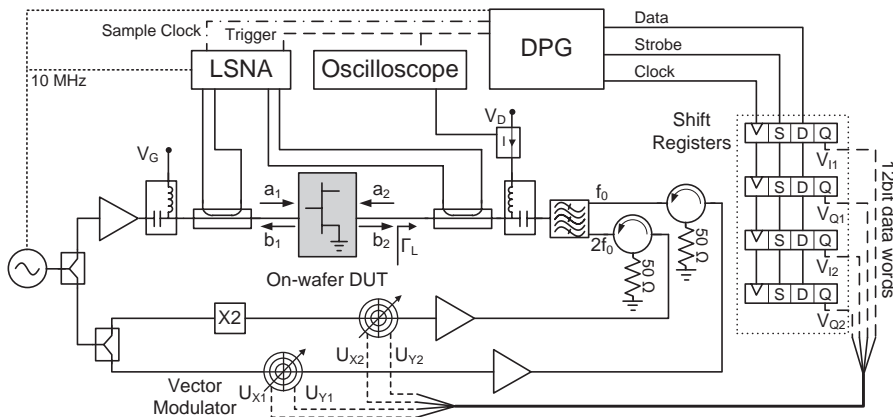


**Figure 3.3:** The multi harmonic active load-pull setup capable of waveform acquisition.

and waveform acquisition capabilities. Both these requirements can be solved by using an LSNA. The LSNA is capable of multi harmonic modulated measurements, hence it fulfils the basic requirements of a fast multi harmonic active load-pull system. The control signals to the vector modulators needs to be synchronised with the LSNA samplers to avoid spectral leakage. The procedure for enabling these synchronised measurements is presented in [b]. The complete multi harmonic active load-pull setup capable of waveform acquisition is shown in Fig. 3.3. The illustrated setup is configured for load-pull on two harmonics, but can easily be extended. Only one signal source is used, and the signal is divided to generate both the drive signal and the injected signals on the load side. The higher order harmonics are generated using frequency doublers and triplers. The samplers in the LSNA and the trigger are controlled using a digital pattern generator (DPG). The DPG also generates the control signals to the vector modulators, enabling fast control of the load impedance, and synchronised measurements.

The fast varying load impedance increases the measurement speed, but adds an additional problem. The drain current depends on the load impedance, hence the current varies fast and the reading obtained from the bias supply is a time average of the drain current. An oscilloscope is therefore included in the setup, with a current probe connected to the drain bias line to measure the dynamic drain current. The oscilloscope is triggered by the DPG, and the measurement software combines the data from both the oscilloscope and the LSNA to reconstruct the voltage and current waveforms.

### 3.1.2 Optimisation routine

One problem with an open loop active load-pull setup is to determine the values of the control signals to the vector modulators. This can be accomplished by pre-calibrating the path of the injected signal to know the amplitude and phase of  $a_2$  at the DUT reference plane [85]. But, the pre-calibration is very sensitive to drift, and the used power amplifiers need to be at a stable temperature and operate in the linear regime. It is therefore beneficial to use an optimisation

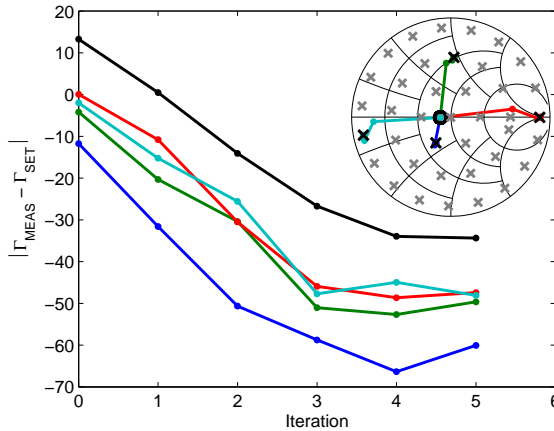


**Figure 3.4:** The error of the optimisation versus number of iterations (black indicates the total error). Inset shows the start (circles) and stop (crosses) values of the load impedances.

based routine, without the need for pre-calibration and the control signals to the vector modulators are determined on the fly. A Newton-Raphson based optimisation algorithm converging within 4 iterations was presented in [88], but the proposed method is limited to the fundamental frequency (i.e. no harmonics). As stated in [89], an iterative procedure is necessary for multi harmonic terminations since the harmonics are coupled to each other, and a change in the load impedance at the second harmonic influences the response at the fundamental frequency. It is therefore necessary to extend the method in [88] to enable multi harmonic optimisation, and an extension to this is presented in [D]. The proposed method makes use of the modulated capabilities of the LSNA to present multiple impedance states during the duration of one measurement. This enables fast measurements of the Jacobian matrix for the optimisation, and also optimisation of multiple impedance states simultaneously. The convergence of the optimisation is shown in Fig. 3.4, where 39 different impedance states are simultaneously optimised, and the optimisation converges within 3 to 5 iterations.

This new optimisation method is a significant improvement compared to other active load-pull setups. The system from Anteverta requires at least 15 iterations before converging according to a video on their website [90], and it appears that an iterative procedure is used for multi harmonic optimisation. The predecessor of the system from Mesuro requires according to [85] at least 15 iterations before it converges.

### 3.1.3 Measurement results

The combination of nonlinear measurements and multi harmonic load-pull gives for example detailed information about the device operation in different amplifier topologies. The extrinsic load lines are measured, and the intrinsic waveforms can be determined by de-embedding the passive components

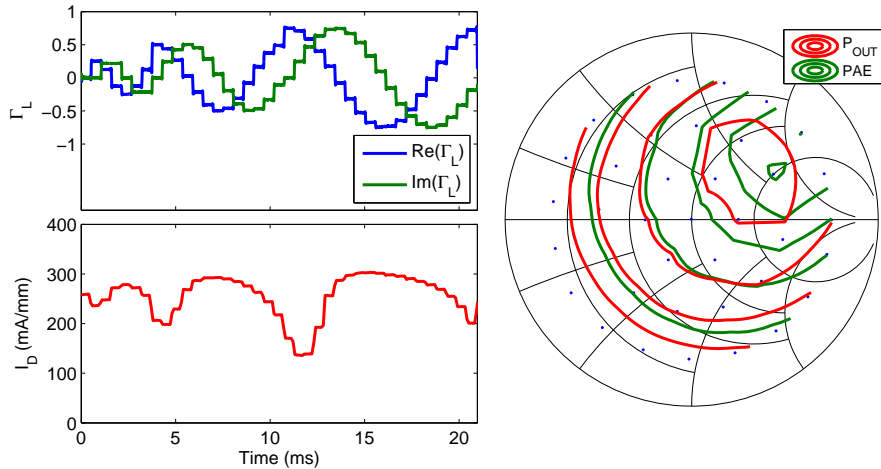


**Figure 3.5:** Active load-pull measurement on a GaN based HEMT. Top: The measured modulated load reflection coefficient with 39 different states within 21 ms. Bottom: The measured drain current during the load-pull characterisation. Right: Output power and PAE contours.

enclosing the nonlinear core of the DUT [91].

The multi harmonic active load-pull setup is used to measure GaN based HEMTs to illustrate the possibilities these load dependent nonlinear characterisations provide. First a standard fundamental load-pull measurement is carried out, shown in Fig. 3.5. The measurement takes 21 ms, and 39 different impedance states are measured, covering almost the entire Smith-chart. The drain current is measured using the current probe and oscilloscope, and its load dependence is clearly shown. This is to date the fastest setup for controlled load-pull measurements with complete waveform acquisition.

The importance of accurate control of the second harmonic is illustrated in Fig. 3.6. The fundamental load impedance is kept constant at the impedance corresponding to the maximum output power. The phase of the load reflection coefficient at the second harmonic is swept around the Smith-chart with a fixed magnitude of 0.8. The efficiency is very sensitive to the angle of  $\Gamma_{2f_0}$ , and a dip occurs at around 30 degrees. This clearly illustrates the importance of full control over the impedances at the higher order harmonics when performing load-pull measurements.

The waveform measurement capabilities are also very useful for device comparison studies. GaN based HEMTs suffer from low frequency dispersion due to trapping. The trapping is due to surface states, and a high quality surface passivation is needed to reduce the influence of these charges. It is therefore necessary to evaluate the influence of different passivations on the RF performance. Low quality surface passivations cause knee-walkout effects, increasing the on-resistance at RF, and hence reducing the output power. The active load-pull setup is very useful for knee-walkout analysis since multiple impedances are measured simultaneously and the entire knee region of the transistor is instantly characterised. The knee-walkout effects on four differ-

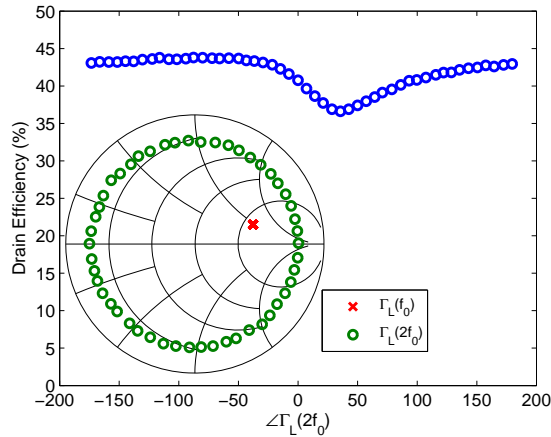


**Figure 3.6:** Power added efficiency versus the phase of the second harmonic load impedance. Insert shows the measured load impedances at the fundamental and second harmonic.

ent GaN HEMTs (three transistors from commercial GaN foundries and one transistor from Chalmers) are shown in Fig. 3.7. It can be seen that the knee-walkout is still a problem for some manufactures, limiting their device performance.

## 3.2 Dynamic load modulation

There is an increasing need to improve the efficiency of amplifiers used for highly modulated signals, such as in mobile communication systems. The higher order modulations results in a high peak to average power ratio of the transmitted signal. Hence, the amplifier needs to be designed for the higher peak output power, but operates most of the time at the average output power for standard amplifier classes of operation (class A, AB, B and C). The average efficiency for modulated signals can therefore be significantly lower than the peak efficiency at maximum output power. The efficiency in back-off can be improved by using advanced topologies such as Chireix [92], Doherty [93], envelope elimination and restoration [94], or dynamic load modulation (DLM) [81].

This section focuses on the DLM topology, consisting of one transistor with a variable matching network. The basic idea in the DLM topology is to keep the voltage swing constant, while the current swing is reduced at back-off operation by changing the load impedance, as illustrated in Fig. 3.8. This improves the efficiency by reducing the power consumption in the transistor at low output power levels.

The load impedance maximising the efficiency, is characterised versus output power by using the active load-pull setup in Section 3.1. Measurements are carried out on a  $10 \times 300 \mu\text{m}$  laterally diffused metal oxide semiconductor (LD-MOS) transistor, and the results are shown in Fig. 3.9. Each combination of  $P_{in}$  and  $Z_L$  is represented by a grey dot, and the load impedances correspond-

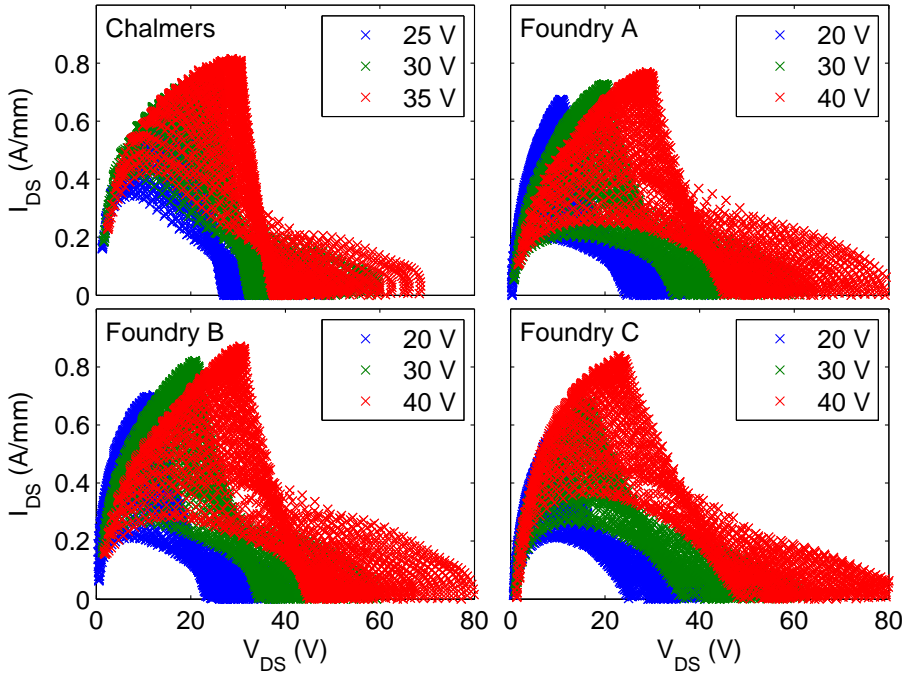


**Figure 3.7:** Study of the knee-walkout on four different manufacturers.

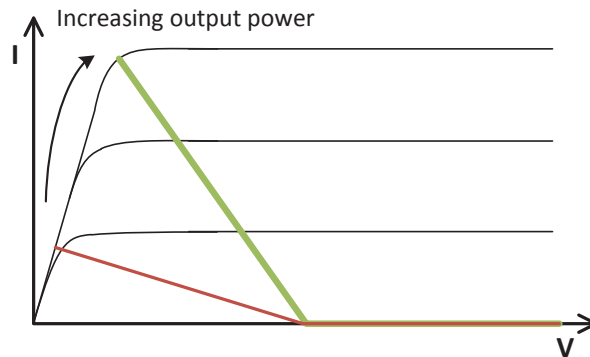


**Figure 3.8:** Illustration of the load modulation principle.

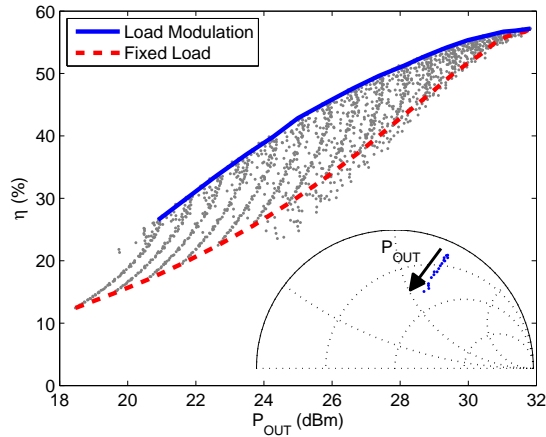


**Figure 3.9:** Drain efficiency versus output power and load impedance. The solid blue line corresponds to the efficiency for the optimum  $\Gamma_L$  trajectory seen in the inset. The dashed red line corresponds to the efficiency in back-off for load impedance at peak efficiency.

ing to the highest efficiency versus output power are shown in the inset as blue dots. It is clear that the optimum impedance is decreasing with increasing output power, which is as predicted from Fig. 3.8. The efficiency in back-off could be improved by more than 10 percentage units by DLM compared to a fixed  $Z_L$  (solid blue line compared to dashed red line).

One problem with the DLM topology is how to implement the variable matching network. Any loss in the load network significantly reduces the efficiency, since it is on the high power side of the transistor. Low loss variable components are therefore needed. The variable load network could be realised by using tuneable elements such as SiC varactors [95], and [n]. The DLM topology has been used in several designs, and the results show increased average efficiency for modulated signals compared to fixed loads [96], and [c]. However, the load network prevents measurements of the waveforms at the device terminals. The transistor waveforms gives detailed information about the device performance, and the presented  $Z_L$  can be calculated. It could therefore be of interest to characterise the transistor under DLM operation independently of the variable matching network.

A new characterisation method for device level DLM measurements is presented in [E], making use of the setup in Section 3.1. The setup presents dynamically varying load impedance, with a modulated signal injected at the input of the transistor. A vector signal generator (VSG) is used to generate the modulated input signal, and the control signals to the vector modulator are controlled using an arbitrary waveform generator (AWG), which is synchronised with the VSG. The load impedance is dynamically controlled by using the AWG with pre-determined control signals. The LD MOS transistor, previously characterised by static load-pull measurements in Fig. 3.9, is used for the evaluation. The load impedance is dynamically controlled, synchronised with the output power, and the results are shown in Fig. 3.10.

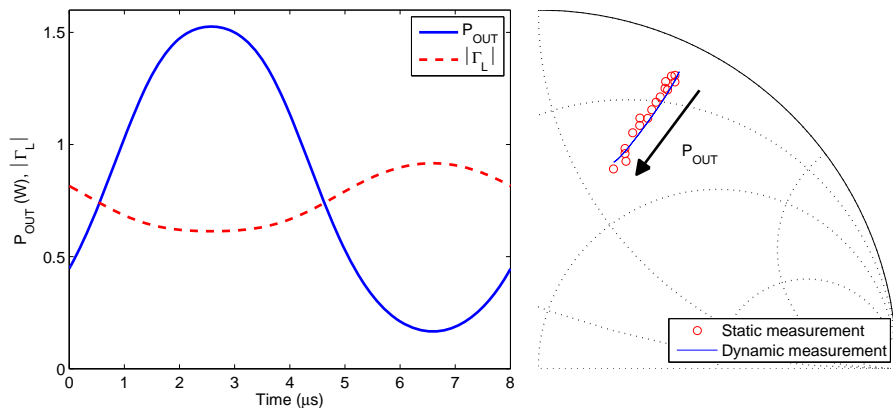


**Figure 3.10:** Dynamic load modulation measurements on a 10x300  $\mu\text{m}$  LDMOS. Left: Time varying  $P_{out}$  and  $|\Gamma_L|$ . Right: Dynamic load impedance compared to optimum trajectory from static measurements.

The time varying  $\Gamma_L$  and  $P_{out}$  are, as aimed for, synchronised. The dynamically varying  $\Gamma_L$  follows the optimum trajectory from the CW characterisation perfectly. The proposed setup gives a fast test of the suitability of a specific transistor for use in DLM topologies. The setup could also be used in the analysis of Doherty amplifiers, which also make use of the load modulation principle. Each path in the Doherty amplifier can be analysed independently by presenting the wanted dynamic load impedance using the vector modulators.

### 3.3 Nonlinear characterisation of SiC varactors

It was shown in Section 3.2 that tunable elements could be very useful to improve the efficiency of amplifiers intended for use with high order modulation signals. Furthermore, there is an increased interest in frequency reconfigurable networks, such as enabling power amplifiers to change its centre frequency for multi band operation. One such tuneable element is the varactor, which is a variable capacitance. The SiC Schottky varactor is studied in this section, but the presented characterisation method is applicable to all types of varactors. The SiC varactor is a Schottky contact in series with an ohmic contact [95], and [n]. The depletion region under the Schottky contact creates the variable capacitance.

The most commonly used figure of merit when comparing varactors (and capacitors) is the Q-factor. The Q-factor is defined as the ratio between the time average stored energy in the system and the energy loss per second. This is usually simplified to:

$$Q_{lin} = \frac{1}{\omega_0 R_{series} C}, \quad (3.2)$$

where  $C$  is the capacitance value, and  $R_{series}$  is the series resistance.

Equation (3.2) is only valid for varactors (capacitors) where  $R_{series}$  and  $C$  are independent of the applied signal, and hence constant. The voltage swing over a varactor used in a DLM amplifier can be twice the operating voltage of the transistor. It is therefore probably not correct to assume linear operation of the varactor due to its nonlinear C(V) characteristics. Hence, it is necessary to derive the Q-factor using other methods. A new characterisation method for varactors under large signal excitation is presented in [G]. The active load-pull setup presented in Section 3.1 is used to control the load impedance of the varactor at both the fundamental and at the second harmonic. The studied varactor is intended for use in a series configuration. A simplified analysis is therefore obtained by short circuiting the fundamental at one of its ports, hence creating a virtual one port device. This effectively removes the influence of the pad capacitances, and allows an accurate study of the intrinsic varactor.

The complex power ( $P_C$ ) flowing into a port of a passive network is according to Maxwell's equations given by:

$$P_C = \frac{VI^*}{2} = P_{loss} + 2j\omega_0 (W_m - W_e), \quad (3.3)$$

where  $P_{loss}$  is the power loss,  $W_m$  the stored magnetic energy, and  $W_e$  the stored electric energy. Hence, the Q-factor is according to its definition given by:

$$Q = \frac{Im(VI^* - 2j\omega_0 W_m)}{Re(VI^*)}. \quad (3.4)$$

The stored magnetic energy needs to be included to remove the influence of the parasitic inductance in the varactor. The Q-factor is therefore directly obtained by measuring the complex port power of the varactor.

Measurements are carried out on a SiC varactor in series, where the fundamental frequency is short circuited at one of the ports. The magnitude of the load reflection coefficient at the second harmonic is set to one, and the phase is swept one revolution around the Smith-chart. The delivered output powers at the first three harmonics are shown in Fig. 3.11.

It can be seen that the harmonic generation resonates at an angle of approximately 158°. This is due to the series resonance of the varactor capacitance with the inductive load corresponding to that angle. The generation of higher order harmonics acts as a loss at the fundamental frequency [97], and hence the Q-factor is reduced at the series resonance, as shown in bottom plot of Fig. 3.11. It is also observed that the delivered output power of the third harmonic is lowest when the second harmonic is terminated in an open circuit. This is related to the voltage-charge (V(Q)) characteristics of the varactor. The V(Q) is almost quadratic for the used SiC varactor, hence the nonlinearity is almost perfectly of second order. The square-law characteristics of the V(Q) limits the generation of voltage harmonics to the second order. The generation of higher order harmonics requires a harmonic current to pass through the varactor. The higher order harmonics are then generated by the mixing between the harmonic current and the excitation at the fundamental. Terminating the second harmonic in an open circuit prevents generation of a second harmonic in the current, and hence no generation of a third harmonic in the voltage is possible [98].

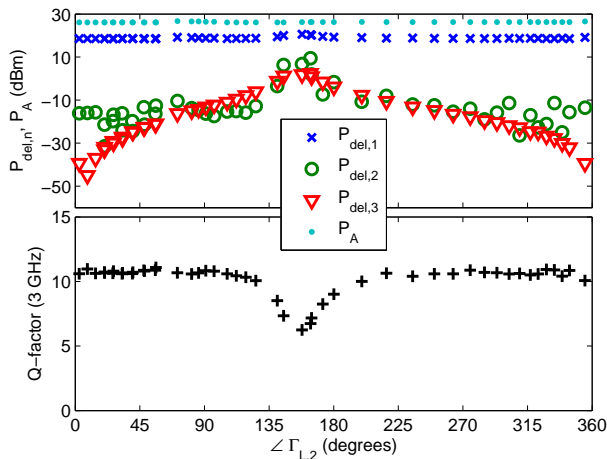


**Figure 3.11:** Multi harmonic load-pull measurement on a SiC varactor. Top: Delivered output power to the load at the first three harmonics versus angle of the load reflection coefficient at the second harmonic. Bottom: Q-factor versus angle of the load reflection coefficient at the second harmonic.

The new characterisation method to determine the Q-factor of a varactor illustrates the importance in taking the nonlinear distortion into account when characterising devices. The harmonic generation affects the varactor operation, and could severely degrade the performance of circuits utilising varactors.

### 3.4 Linear approximation

Exiting a nonlinear system (with at least a second order term) with a modulated signal will generate higher order harmonics and a response around DC. The response at DC excites the memory effects, and can create nonlinear distortion at the excitation frequency. These effects are not included in linear characterisation methods, such as S-parameters, and hence a nonlinear equivalent or model is needed.

There are several solutions to characterise and model nonlinear devices. One of these is the PHD model [31]. The PHD model can be seen as an extension of the S-parameters, taking into account the coupling between the harmonics. The model is table based, and hence needs extensive measurements to be useful. Due to this, it predicts gain compression and waveforms with high accuracy, but the model is only valid for narrow bandwidth excitations. This implies that nonlinear distortion due to memory effects is not included, and that simulation results for modulated input signals can be invalid. This problem is partly solved by an extension to the PHD model proposed in [99], which includes nonlinear distortion due to memory effects. However, the extraction method does not provide any measure of the validity of the model.

Another solution is to use a linear approximation to describe the nonlinear device. The linear approximation used in this thesis is based on the best

linear approximation (BLA) [100]. The BLA can be seen as a large signal S-parameter representation, valid for signals having their power spectral density in common with the excitation signal ( $U$ ) used during the extraction, and are part of the Gaussian noise class of signals. The frequency dependence of the system and the level of the nonlinear distortion are directly visualised by the BLA. It is therefore possible to directly determine if the linear approximation can be trusted, or if a nonlinear model is necessary to correctly predict the response of the system. The output spectrum ( $Y$ ) from the nonlinear DUT is given by:

$$Y(f) = G_{BLA}(f)U(f) + Y_S(f) + N_S(f), \quad (3.5)$$

where  $G_{BLA}(f)$  is the frequency dependent best linear approximation. The in-band distortion generated due to odd order nonlinearities, and can be separated into two parts, The coherent part, acting as bias on the BLA, and the non-coherent part, acting as a stochastic contribution modelled by a Gaussian noise source ( $Y_S(f)$ ). The extraction is measurement based, and hence the random errors in the measurement setup acts as Gaussian distributed measurement noise ( $N_S(f)$ ). The validity of the BLA is obtained by calculating the sample variance of both the measurement noise, and the non-coherent contribution due to the nonlinear distortion. These figures gives an indication of the level of the nonlinear distortion, and give a quality measure of the extracted linear approximation.

It is possible to measure the level of the in-band distortion, classify the nonlinearities in even and odd order, estimate the non-coherent contributions, and estimate the measurement noise by extracting the BLA. The extraction of the BLA is simplified by the use of multitone excitation signals. The measurement procedure is described in detail in [101], and the excitation signals are described in [102]. The used test signals are random phase multisines, which are part of the Gaussian noise class of signals. Only the odd bins are excited and this allows for a classification of the nonlinearities into even and odd contributions. This is due to the fact that even nonlinearities transfer power to the even frequencies and the odd nonlinearities transfer power to the odd frequencies (when using excitation signals with power only at the odd bins). Hence, the level of the even nonlinearities is directly obtained from the even bins in  $Y$ . The odd bins of  $Y$  contain both the linear response of the system and the nonlinear distortion due to odd order nonlinearities. It is therefore necessary to generate an excitation signal where randomly odd bins are left unexcited. These unexcited bins will act as detection lines, and the level of both the even and the odd nonlinearities can be estimated.

Since the BLA approximates the linear response of the system, no information about memory effects is given. The memory effects are excited and are indirectly included in the BLA extraction. this is due to that the even order nonlinearities generates a response at DC, and hence excites the slow memory effects. An extension of the BLA framework is therefore necessary to allow for the study of the memory effects in detail.

### 3.4.1 Extending the BLA

The BLA framework is extended in [F] to include second order nonlinearities, and hence enable the analysis of low frequency dispersion effects. The standard BLA is used as the starting point for the extension. This implies that the nonlinear system must fulfil the same requirements as in [100]. The system needs to be period conserving (no generation of subharmonics), and the excitation signals are required to be part of the Gaussian noise class of signals.

An ideal second order nonlinear system generates a response both at DC and at  $2f_0$ , and the extended BLA gives a measure on how close the measured system is to that ideal second order system. This is accomplished by using the squared time domain excitation signal as the reference signal in the calculation of the extended BLA. This corresponds to a convolution in the frequency domain, and the extended BLA, taking into account both the linear ( $G_1$ ) and quadratic ( $G_2$ ) parts, is given by:

$$Y = G_1 U + G_2 U * U, \quad (3.6)$$

where  $*$  is the convolution operator.

The used measurement system is the LSNA, and the output from it is the spectrum around each harmonic with a maximum bandwidth of 20 MHz. The entire spectrum is not available, and the formulation in (3.6) is therefore not directly usable for the output from the LSNA. The calculation of the extended BLA is reformulated to be useful with the LSNA by treating each harmonic separately, according to:

$$\begin{aligned} \begin{bmatrix} Y_{DC} \\ Y_{f_0} \\ Y_{2f_0} \end{bmatrix} &= \begin{bmatrix} G_{11} & 0 \\ 0 & G_{12} \\ 0 & 0 \end{bmatrix} \begin{bmatrix} U_{DC} \\ U_{f_0} \end{bmatrix} \\ &+ \begin{bmatrix} G_{21} & 0 & 0 \\ 0 & G_{22} & 0 \\ 0 & 0 & G_{23} \end{bmatrix} \begin{bmatrix} 2U_{f_0}^* * U_{f_0} \\ 2U_{DC} * U_{f_0} \\ U_{f_0} * U_{f_0} \end{bmatrix}, \end{aligned} \quad (3.7)$$

The nonlinear distortion affects the extended BLA in the same way as the standard BLA. The coherent contribution, due to even order nonlinearities, acts as bias, and the non-coherent contributions acts as Gaussian noise. The estimation of the non-coherent contributions and the measurement noise follows the same procedure as for the standard BLA by measuring multiple realisations, and several consecutive periods of the excitation signal.

### 3.4.2 Extended BLA measurements

A nonlinear measurement setup, capable of measuring the modulated spectrum at DC and at the harmonics is needed to extract the extended BLA. The measurement of the harmonics relies on a synchronised acquisition, hence the harmonics needs to be measured using a common time reference. Furthermore, the low frequency spectrum needs to be captured to study the low frequency dispersion. The system used in this thesis is the LSNA, with a low frequency test-set extension (NM500, NMDG NV). The setup enables measurement of the low frequency spectrum between 10 kHz and 20 MHz, and simultaneously

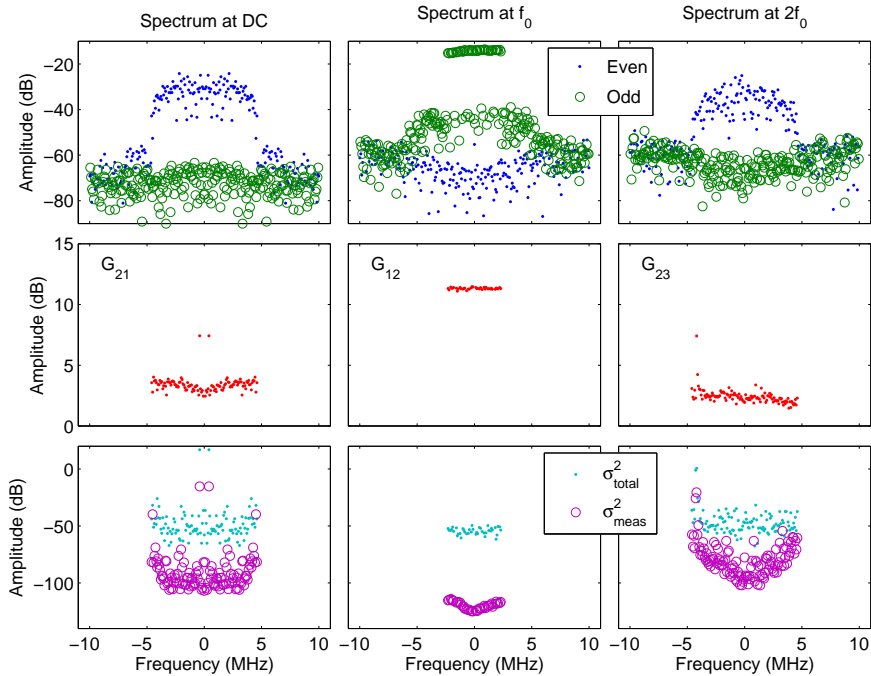


**Figure 3.12:** Measurement results of the GaN HEMT when applying an excitation at the RF port. Top row from left to right: The odd and even bins of the output spectrum at DC,  $f_0$  and  $2f_0$ . Middle row from left to right:  $G_{21}$ ,  $G_{12}$ , and  $G_{23}$ . Bottom row from left to right: The measurement and total noise variances for  $G_{21}$ ,  $G_{12}$ , and  $G_{23}$  respectively.

measures the harmonics with a modulation bandwidth of up to 20 MHz. The low frequency test-set also supports injection of modulated bias voltages, hence enabling low frequency load-pull measurements.

Measurements are carried out on a  $2 \times 100 \mu\text{m}$  wide GaN HEMT to demonstrate the possibilities with the extended BLA. The GaN HEMT is biased at a class AB operating point with 20 V on drain. The RF output is terminated in  $50 \Omega$ , which is not optimum in terms of power handling. A 5 MHz wide random phase multisine with an average power of 3 dBm is injected at the input of the HEMT. This corresponds to the 1 dB compression point for the mismatched DUT. The measured output spectrum around DC,  $f_0$ , and  $2f_0$  are shown in Fig. 3.12.

The measured spectrum at DC looks noisy, but the calculated  $G_{21}$  show a relatively flat response, with a small frequency dependence. The two dots at around 100 kHz offset are due to a resonance in the used bias tees. The frequency dependence seen in the variance of the measurement noise at DC and  $2f_0$  is due to the convolution of the signal at  $f_0$ . The convolution results in that more power is concentrated to the centre of the band, and less power is present at the band edges of the spectrum. This results in a worse signal to noise ratio at the band edges, and hence an increase in  $\sigma_{meas}^2$ . Furthermore, the level of  $\sigma_{total}^2$  at 100 kHz offset is in the same order of magnitude as  $G_{21}$

due to the resonance in the bias tee. This indicates that  $G_{21}$  is not valid for these frequencies. This information is not known without the calculation of  $\sigma_{total}^2$ , which illustrates the advantage of the BLA framework.

The extended BLA opens up new possibilities in device characterisation. Low frequency memory effects can be directly visualised by studying the frequency response of  $G_{21}$ , and the validity of the BLA is given by calculating  $\sigma_{meas}^2$  and  $\sigma_{total}^2$ .



# Chapter 4

## Summary of appended papers

### Paper A

#### **Electrothermal Access Resistance Model for GaN Based HEMTs**

The electrothermal properties of the access resistances in GaN based HEMTs was thoroughly studied. A new model for the electron transport was proposed, extending the commonly used Caughey-Thomas model. Furthermore a new method for isothermal characterisation was proposed, using an LSNA. This also enabled the calculation of the channel temperature.

The theory behind the modelling was a joint effort by the writers, and the author did the measurements, modelling and writing of the paper.

### Paper B

#### **Thermal Study of the High-Frequency Noise in GaN HEMTs**

The temperature dependence of the noise parameters in GaN based HEMTs was thoroughly studied in this paper. The major limiting factor was found to be the temperature dependent access resistances.

The measurements, modelling and writing of the paper were done by the author.

### Paper C

#### **An X-Band AlGaIn/GaN MMIC Receiver Front-End**

An integrated receiver front-end in GaN working at X-band was presented in this paper. This showed the potential for GaN to be used in monolithic transceiver front-ends.

The design was a joint effort between Saab and the author, and the writing was carried out by the author.

## Paper D

### **Fast Multi Harmonic Active Load-Pull System With Waveform Measurement Capabilities**

A new multi harmonic load pull setup was presented. It was faster than existing commercial systems, and the convergence of the optimisation routine was a significant improvement.

The author constructed the measurement setup and wrote the paper.

## Paper E

### **Characterization Setup for Device Level Dynamic Load Modulation Measurements**

A new application for active load-pull systems was presented in this paper, which allowed for dynamic load modulation of a transistor.

The author built the setup, did the measurements and the writing of the paper.

## Paper F

### **Extending the Best Linear Approximation to Characterize the Non-linear Distortion in GaN HEMTs**

The BLA was extended in this paper to enable the analysis of low frequency distortion in especially GaN based HEMTs.

This was a joint publication between Chalmers University of Technology, Vrije Universiteit Brussel, and NMDG NV. The theory was developed by Yves Rolain and the author. The measurements and the writing of the paper were carried out by the author.

## Paper G

### **Nonlinear Characterization of Varactors for Tunable Networks by Active Source-Pull and Load-Pull**

A new nonlinear characterisation method was presented in this paper, allowing for the extraction of the Q-factor under large signal excitation.

This paper was a team effort, and the author contributed to the measurement setup and the theory of the data analysis.

# Chapter 5

## Conclusions

This thesis has focused on some of the problems related to characterisation of high power density devices like GaN based HEMTs, as well as the possibilities given by the new nonlinear measurement systems.

The large self-heating observed in GaN based HEMTs is often not considered as an issue in device characterisation, as shown with the many papers regarding nonlinear access resistances due to bias dependence. The access resistances are indeed bias dependent, as shown in this thesis, but the effects of self-heating at low electric fields is significantly larger. It is therefore necessary to take the self-heating into account during the device characterisation. The nonlinear distortion due to self-heating needs to be included in the models for correct prediction of the response to modulated signals. Furthermore, correctly estimated operation temperature enables better estimations of the reliability (such as MTTF).

The first steps towards a monolithically integrated transceiver were taken. The high power capabilities have been verified for the GaN based HEMT, but the robustness and low noise properties need further studies. A monolithically integrated GaN based transceiver could, even with inferior low noise performance, replace existing solutions due to the reduce weight and size. The noise performance at a system level is however comparable to GaAs pHEMT due to the possibility to remove or simplify protective limiters. The GaN based HEMT is therefore an excellent candidate for high power and high efficiency transmitters as well as robust and linear receivers.

The use of nonlinear measurement systems is increasing, and there exists several commercial actors delivering these instruments. The manufactures promises that the nonlinear measurement systems do everything for you by pressing a button. This is in some cases true, but in most cases the user needs to put in a lot of knowledge into the measurement. For example, how do you know that the extracted PHD model is valid for the used excitation in the simulation? These nonlinear measurement systems give many possibilities, and some new characterisation methods were presented in this thesis. Significantly faster characterisations are possible by utilising the modulated capabilities when performing load-pull measurements. Amplifier topologies could directly be tested directly with the transistor without the need to manufacture circuits. Memory effects due to large signal excitations can be directly

visualised. As shown, the number of applications for nonlinear measurement systems is increasing by the day. Nonlinear measurements should be part of the standard device characterisation, and could possibly replace both the IV and S-parameter measurements. But most importantly, the users most know when the measured results or the extracted models could be trusted or not.

## 5.1 Future work

Several of the topics treated in this thesis are in need of continued research. These are as follows:

- Monte Carlo simulations indicate that the differential resistance at high electric fields is negative in the AlGa<sub>N</sub>/Ga<sub>N</sub> 2DEG. This still needs to be verified with measurements, and could potentially be utilised for frequency generation purposes, like the Gunn diode. The proposed isothermal characterisation method could be a good starting point. The next step is to control the temperature by either cooling the DUT or using a pulsed setup.
- The first steps towards a monolithically integrated GaN based transceiver front-end were taken in this thesis. However, there is still need to demonstrate a fully functional high power transceiver, withstanding very high input powers. The performance at a system level could very well outperform a GaAs pHEMT based transceiver. But more importantly, the extremely small size due to the monolithically integrated transceiver would allow more modules to be used, and hence improved performance for active electronically scanned array systems.
- The low noise performance of the AlGa<sub>N</sub>/Ga<sub>N</sub> HEMT showed large temperature dependence. It is therefore interesting to further characterise the low noise properties at cryogenic temperatures for optimised layouts and material compositions. The very high  $f_T$  and  $f_{max}$  figures of 260 and 400 GHz respectively should improve the low noise performance. Maybe GaN based HEMTs could be an option for low noise applications at cryogenic temperatures.
- The presented extension to the BLA framework enables characterisation of low frequency dispersion due to memory effects. Due to the limited bandwidth of the measurement system, no dynamics were observed in the down conversion. According the frequency response characterisation of the thermal impedance, a system capable of capturing the spectrum from DC up to at least 100 MHz is needed.
- There is a need for a nonlinear version of the S-parameters to minimise the step from VNA measurements to nonlinear characterisation, and the PHD model is a good starting point. However the user cannot tell whether or not the model is valid for the used excitation. The BLA framework gives the validity of the approximation, but does not include harmonic generation.

# Acknowledgment

This work would never have happened without the help and support from several persons. Therefore I would like to express my gratitude to those who have supported my work.

I would like to thank my examiner Prof. Herbert Zirath for giving me the opportunity to work and perform my research at the Microwave Electronics Laboratory.

My research has been carried out in the GigaHertz Centre, which is a great collaboration between Chalmers and world leading companies within the microwave field. I would therefore like to thank Prof. Jan Grahn for his fantastic work in creating this great research environment.

I would also like to thank my supervisors, Dr. Niklas Rorsman for a great support and endless work in the cleanroom, and Dr. Kristoffer Andersson for all guidance, support, great discussions, and for always taking the time when needed.

I had a very nice research visit at department ELEC at the Vrije Universiteit Brussel, and I would like to thank Prof. Johan Schoukens for letting me come to them. I would also like to thank Prof. Yves Rolain for the great visit, and all the interesting discussions. Furthermore, I would like to thank the entire ELEC group for the good time I had down there.

The research in this thesis relies intensively on the work done by the MWBG group. I would therefore like to thank the entire group for the great job in the cleanroom with the GaN HEMT and GaN MMIC fabrications. A special thanks to all my co-authors, without your contributions and support, this would not have happened. I would finally like to thank all of the people working at MEL for creating a great and inspiring research environment.

This research has been carried out in the GigaHertz Centre in a joint research project financed by Swedish Governmental Agency of Innovation Systems (VINNOVA), Chalmers University of Technology, Comheat Microwave AB, Ericsson AB, Infineon Technologies Austria AG, Mitsubishi Electric Corporation, NXP Semiconductors BV, Saab AB, and SP Technical Research Institute of Sweden.



# Bibliography

- [1] M. Asif Khan, J. N. Kuznia, J. M. Van Hove, N. Pan, and J. Carter, "Observation of a two-dimensional electron gas in low pressure metalorganic chemical vapor deposited GaN-Al<sub>x</sub>Ga<sub>1-x</sub>N heterojunctions," *Appl. Phys. Lett.*, vol. 60, no. 24, pp. 3027–3029, Jun. 1992.
- [2] M. Asif Khan, A. Bhattarai, J. N. Kuznia, and D. T. Olson, "High electron mobility transistor based on a GaN-Al<sub>x</sub>Ga<sub>1-x</sub>N heterojunction," *Appl. Phys. Lett.*, vol. 63, no. 9, pp. 1214–1215, Aug. 1993.
- [3] U. K. Mishra, S. Likun, T. E. Kazior, and Y.-F. Wu, "GaN-Based RF Power Devices and Amplifiers," *Proc. IEEE*, vol. 96, no. 2, pp. 287–305, Feb. 2008.
- [4] M. Asif Khan, J. N. Kuznia, D. T. Olson, W. J. Schaff, J. W. Burm, and M. S. Shur, "Microwave performance of a 0.25 μm gate AlGaN/GaN heterostructure field effect transistor," *Appl. Phys. Lett.*, vol. 65, no. 9, pp. 1121–1123, Aug. 1994.
- [5] Y.-F. Wu, B. P. Keller, S. Keller, D. Kapolnek, S. P. Denbaars, and U. K. Mishra, "Measured microwave power performance of AlGaN/GaN MODFET," *IEEE Electron Device Lett.*, vol. 17, no. 9, pp. 455–457, Sep. 1996.
- [6] K. Shinohara, D. Regan, I. Milosavljevic, A. L. Corrion, D. F. Brown, P. J. Willadsen, C. Butler, A. Schmitz, S. Kim, V. Lee, A. Ohoka, P. M. Asbeck, and M. Micovic, "Electron Velocity Enhancement in Laterally Scaled GaN DH-HEMTs With  $f_T$  of 260 GHz," *IEEE Electron Device Lett.*, vol. 32, no. 8, pp. 1074–1076, Aug. 2011.
- [7] Y.-F. Wu, M. Moore, A. Saxler, T. Wisleder, and P. Parikh, "40-W/mm Double Field-plated GaN HEMTs," in *64th Device Research Conference Digest*, Jun. 2006, pp. 151–152.
- [8] M. Asif Khan, M. S. Shur, J. N. Kuznia, Q. Chen, J. Burm, and W. Schaff, "Temperature activated conductance in GaN/AlGaN heterostructure field effect transistors operating at temperatures up to 300 °C," *Appl. Phys. Lett.*, vol. 66, no. 9, pp. 1083–1085, Feb. 1995.
- [9] M. Asif Khan, Q. Chen, M. S. Shur, B. T. Dermott, J. A. Higgins, J. Burm, W. Schaff, and L. F. Eastman, "[short-channel gan/aigan doped channel heterostructure field effect transistors with 36.1 cutoff freq," *Electron Lett.*

- [10] Y.-F. Wu, B. P. Keller, S. Keller, N. X. Nguyen, M. Le, C. Nguyen, T. J. Jenkins, L. T. Kehias, S. P. Denbaars, and U. K. Mishra, "Short channel AlGaIn/GaN MODFET's with 50-GHz  $f_T$  and 1.7-W/mm output-power at 10 GHz," *IEEE Electron Device Lett.*, vol. 18, no. 9, pp. 438–440, Sep. 1997.
- [11] U. K. Mishra, Y.-F. Wu, B. P. Keller, S. Keller, and S. P. Denbaars, "GaN microwave electronics," *IEEE Trans. Microw. Theory Tech.*, vol. 46, no. 6, pp. 756–761, Jun. 1998.
- [12] W. Lu, J. Yang, M. A. Khan, and I. Adesida, "AlGaIn/GaN HEMTs on SiC with over 100 GHz  $f_T$  and low microwave noise," *IEEE Trans. Electron Devices*, vol. 48, no. 3, pp. 581–585, Mar. 2001.
- [13] T. Palacios, A. Chakraborty, S. Heikman, S. Keller, S. DenBaars, and U. Mishra, "AlGaIn/GaN high electron mobility transistors with InGaIn back-barriers," *IEEE Electron Device Lett.*, vol. 27, no. 1, pp. 13–15, Jan. 2006.
- [14] K. Shinohara, A. Corrión, D. Regan, I. Milosavljevic, D. Brown, S. Burnham, P. J. Willadsen, C. Butler, A. Schmitz, D. Wheeler, A. Fung, and M. Micovic, "220GHz  $f_T$  and 400GHz  $f_{max}$  in 40-nm GaN DH-HEMTs with re-grown ohmic," in *IEDM Meeting Tech. Dig.*, Dec. 2010.
- [15] Y.-F. Wu, B. P. Keller, P. Fini, S. Keller, T. J. Jenkins, L. T. Kehias, S. P. Denbaars, and U. K. Mishra, *[IEEE]*.
- [16] Y.-F. Wu, D. Kapolnek, J. Ibbetson, N.-Q. Zhang, P. Parikh, B. P. Keller, and U. K. Mishra, "High Al-content AlGaIn/GaN HEMTs on SiC substrates with very high power performance," in *IEDM Meeting Tech. Dig.*, 1999, pp. 925–927.
- [17] Y.-F. Wu, P. M. Chavarkar, M. Moore, P. Parikh, and U. K. Mishra, "Bias-dependent performance of high-power AlGaIn/GaN HEMTs," in *IEDM Meeting Tech. Dig.*, 2001.
- [18] Y. Ando, Y. Okamoto, K. Hataya, T. Nakayama, H. Miyamoto, T. Inoue, and M. Kuzuhara, "12 W/mm recessed-gate AlGaIn/GaN heterojunction field-plate FET," in *IEDM Meeting Tech. Dig.*, Dec. 2003.
- [19] Y.-F. Wu, A. Saxler, M. Moore, R. P. Smith, S. Sheppard, P. M. Chavarkar, T. Wisleder, U. K. Mishra, and P. Parikh, "30-W/mm GaN HEMTs by field plate optimization," *IEEE Electron Device Lett.*, vol. 25, no. 3, pp. 117–119, Mar. 2004.
- [20] C. Inc. (2011). [Online]. Available: <http://www.cree.com>
- [21] T. S. Inc. (2011). [Online]. Available: <http://www.triquint.com>
- [22] A. Brown, K. Brown, J. Chen, K. C. Hwang, N. Koliás, and R. Scott, "W-Band GaN Power Amplifier MMICs," in *IEEE MTT-S Int. Microw. Symp. Dig.*, Jun. 2011.

- [23] W. Marsetz, A. Hulsmann, K. Kohler, M. Demmler, and M. Schlechtweg, "GaAs PHEMT with 1.6 W/mm output power density," *Electron. Lett.*, vol. 35, no. 9, pp. 748–749, Apr. 1999.
- [24] D. Rytting, "ARFTG 50 year network analyzer history," in *IEEE MTT-S Int. Microw. Symp. Dig.*, Jun. 2008, pp. 11–18.
- [25] H. P. Corp., *Transistor Parameter Measurements*, ser. Application Note 77-1, 1967.
- [26] U. Lott, "Measurement of magnitude and phase of harmonics generated in nonlinear microwave two-ports," *IEEE Trans. Microw. Theory Tech.*, vol. 37, no. 10, pp. 1506–1511, Oct. 1989.
- [27] T. van den Broeck, "Calibrated measurements of nonlinearities in narrowband amplifiers applied to intermodulation and cross modulation compensation," in *IEEE MTT-S Int. Microw. Symp. Dig.*, vol. 3, May 1995, pp. 1155–1158.
- [28] Agilent. (2011) Agilent — PNA-X Series Nonlinear Vector Network Analyzer (NVNA). [Online]. Available: <http://www.agilent.com/find/nvna>
- [29] NMDG. (2011) NMDG. [Online]. Available: <http://www.nmdg.be>
- [30] HFE. (2011) HFE, High Frequency Engineering. [Online]. Available: <http://www.hfemicro.com>
- [31] D. E. Root, J. Verspecht, D. Sharrit, J. Wood, and A. Cognata, "Broadband poly-harmonic distortion (PHD) behavioral models from fast automated simulations and large-signal vectorial network measurements," *IEEE Trans. Microwave Theory Tech.*, vol. 53, no. 11, pp. 3656–3664, 2005.
- [32] G. Simpson, J. Horn, D. Gunyan, and D. E. Root, "Load-pull + NVNA = enhanced X-parameters for PA designs with high mismatch and technology-independent large-signal device models," in *72nd IEEE ARFTG Conf. Dig.*, Dec. 2008, pp. 88–91.
- [33] H. Mnif, T. Zimmer, J. L. Battaglia, and B. Ardouin, "Modeling the self-heating effect in SiGe HBTs," 2002, pp. 96–99.
- [34] T. Palacios, S. Rajan, A. Chakraborty, S. Heikman, S. Keller, S. P. DenBaars, and U. K. Mishra, "Influence of the dynamic access resistance in the  $g_m$  and  $f_T$  linearity of AlGaIn/GaN HEMTs," *IEEE Trans. Electron Devices*, vol. 52, no. 10, pp. 2117–2123, Oct. 2005.
- [35] R. J. Trew, Y. Liu, L. Bilbro, W. Kuang, R. Vetury, and J. Shealy, "Nonlinear source resistance in high-voltage microwave AlGaIn/GaN HFETs," *IEEE Trans. Microw. Theory Tech.*, vol. 54, no. 5, pp. 2061–2067, May 2006.
- [36] D. W. DiSanto and C. R. Bolognesi, "At-Bias Extraction of Access Parasitic Resistances in AlGaIn/GaN HEMTs: Impact on Device Linearity and Channel Electron Velocity," *IEEE Trans. Electron Devices*, vol. 53, no. 12, pp. 2914–2919, Dec. 2006.

- [37] I. Khalil and W. Heinrich, "Influence of Dynamic Access Resistances on the Linearity of Large GaN HEMT Powerbars," *IEEE Microw. Wireless Compon. Lett.*, vol. 19, no. 8, pp. 527–529, Aug. 2009.
- [38] G. Dambrine, A. Cappy, F. Heliodore, and E. Playez, "A new method for determining the FET small-signal equivalent circuit," *IEEE Trans. Microw. Theory Tech.*, vol. 36, no. 7, pp. 1151–1159, Jul. 1988.
- [39] R. Gaska, J. W. Yang, A. Osinsky, C. Q., M. Asif Khan, O. A. O., S. G. L., and S. M. S., "Electron transport in AlGaIn/GaN heterostructures grown on 6H-sic substrates," *App. Phys. Lett.*, vol. 72, no. 6, pp. 707–709, Feb. 1998.
- [40] I. Daumiller, C. Kirchner, M. Kamp, K. J. Ebeling, and E. Kohn, "Evaluation of the temperature stability of AlGaIn/GaN heterostructure FETs," *IEEE Electron Device Lett.*, vol. 20, no. 9, pp. 448–450, Sep. 1999.
- [41] C. H. Oxley, M. J. Uren, A. Coates, and D. G. Hayes, "On the temperature and carrier density dependence of electron saturation velocity in an AlGaIn/GaN HEMT," *IEEE Trans. Electron Devices*, vol. 53, no. 3, pp. 565–567, Mar. 2006.
- [42] Nidhi, T. Palacios, A. Chakraborty, S. Keller, and U. Mishra, "Study of Impact of Access Resistance on High-Frequency Performance of AlGaIn/GaN HEMTs by Measurements at Low Temperatures," *IEEE Electron Device Lett.*, vol. 27, no. 11, pp. 877–880, Nov. 2006.
- [43] T. H. Yu and K. F. Brennan, "Monte Carlo calculation of two-dimensional electron dynamics in GaN-AlGaIn heterostructures," *J. Appl. Phys.*, vol. 91, no. 6, pp. 3730–3736, 2002.
- [44] B. Benbakhti, A. Soltani, K. Kalna, M. Rousseau, and J.-C. De Jaeger, "Effects of Self-Heating on Performance Degradation in AlGaIn/GaN-Based Devices," *IEEE Trans. Electron Devices*, vol. 56, no. 10, pp. 2178–2185, Oct. 2009.
- [45] R. J. T. Simms, J. W. Pomeroy, M. J. Uren, T. Martin, and M. Kuball, "Channel Temperature Determination in High-Power AlGaIn/GaN HFETs Using Electrical Methods and Raman Spectroscopy," *IEEE Trans. Electron Devices*, vol. 55, no. 2, pp. 478–482, Feb. 2008.
- [46] Y. R. Wu and J. Singh, "Transient study of self-heating effects in AlGaIn/GaN HFETs: Consequence of carrier velocities, temperature, and device performance," *J. Appl. Phys.*, vol. 101, no. 11, 2007.
- [47] W. Schokley, "Research and investigation of inverse epitaxial UHF power transistors," Tech. Rep. No. AL TDR 64-207, Air Force Avionics Lab., Wright-Patterson Air Force Base, OH, Tech. Rep., Sep. 1964.
- [48] L. Ardaravičius, A. Matulionis, J. Liberis, O. Kiprijanovic, M. Ramonas, L. F. Eastman, J. R. Shealy, and A. Vertiatchikh, "Electron drift velocity in AlGaIn/GaN channel at high electric fields," *App. Phys. Lett.*, vol. 83, no. 19, pp. 4038–4040, 2003.

- [49] K. Andersson, C. Fager, and J. C. Pedro, "A general procedure for extraction of bias dependent dynamic self heating model parameters," in *IEEE MTT-S Int. Microw, Symp. Dig.*, Jun. 2005.
- [50] R. Ostermeir, K. Brunner, G. Abstreiter, and W. Weber, "Temperature distribution in Si-MOSFETs studied by micro-Raman spectroscopy," *IEEE Trans. Electron Devices*, vol. 39, no. 4, pp. 858–863, Apr. 1992.
- [51] M. Kuball, J. M. Hayes, M. J. Uren, I. Martin, J. C. H. Birbeck, R. S. Balmer, and B. T. Hughes, "Measurement of temperature in active high-power AlGa<sub>N</sub>/Ga<sub>N</sub> HFETs using Raman spectroscopy," *IEEE Electron Device Lett.*, vol. 23, no. 1, pp. 7–9, Jan. 2002.
- [52] G. C. Albright, J. A. Stump, J. D. McDonald, and H. Kaplan, "True temperature measurements on microscopic semiconductor targets," in *Proc. SPIE Thermosense XXI*, vol. 3700, 1999, pp. 245–249.
- [53] A. Sarua, H. Ji, M. Kuball, M. J. Uren, T. Martin, K. P. Hilton, and R. S. Balmer, "Integrated micro-Raman/infrared thermography probe for monitoring of self-heating in AlGa<sub>N</sub>/Ga<sub>N</sub> transistor structures," *IEEE Trans. Electron Devices*, vol. 53, no. 10, pp. 2438–2447, Oct. 2006.
- [54] D. M. Caughey and R. E. Thomas, "Carrier mobilities in silicon empirically related to doping and field," *Proc. IEEE*, vol. 55, no. 12, pp. 2192–2193, Dec. 1967.
- [55] N. X. Nguyen, M. Micovic, W.-S. Wong, P. Hashimoto, P. Janke, D. Harvey, and C. Nguyen, "Robust low microwave noise Ga<sub>N</sub> MODFETs with 0.60 dB noise figure at 10 GHz," *Electron. Lett.*, vol. 36, no. 5, pp. 469–471, Mar. 2000.
- [56] P. Parikh, Y. Wu, M. Moore, P. Chavarkar, U. Mishra, R. Neidhard, L. Kehias, and T. Jenkins, "High linearity, robust, AlGa<sub>N</sub>-Ga<sub>N</sub> HEMTs for LNA and receiver ICs," in *Proc. IEEE Lester Eastman Conf. High-Performance Devices*, Aug. 2002, pp. 415–421.
- [57] S. Nuttinck, E. Gebara, J. Laskar, and M. Harris, "High-frequency noise in AlGa<sub>N</sub>/Ga<sub>N</sub> HFETs," *IEEE Microwave Wireless Compon. Lett.*, vol. 13, no. 4, pp. 149–151, Apr. 2003.
- [58] K. W. Kobayashi, Y.-C. Chen, I. Smorchkova, B. Heying, W.-B. Luo, W. Sutton, M. Wojtowicz, and A. Oki, "A Cool, Sub-0.2 dB Noise Figure Ga<sub>N</sub> HEMT Power Amplifier With 2-Watt Output Power," *IEEE J. Solid-State Circuits*, vol. 44, no. 10, pp. 2648–2654, Oct. 2009.
- [59] H. Nyquist, "Thermal Agitation of Electric Charge in Conductors," *Phys. Rev.*, vol. 32, no. 1, pp. 110–113, Jul. 1928.
- [60] H. Rothe and W. Dahlke, "Theory of noisy fourpoles," *Proc. of the IRE*, vol. 44, no. 6, pp. 811–818, Jun. 1956.
- [61] R. Lane, "The determination of device noise parameters," *Proc. IEEE*, vol. 57, no. 8, pp. 1461–1462, Aug. 1969.

- [62] V. Adamian, "2-26.5 GHz On-Wafer Noise and S-Parameter Measurements Using a Solid State Tuner," in *34th IEEE ARFTG Conf. Dig.*, vol. 16, Nov. 1989, pp. 33–40.
- [63] R. A. Pucel, W. Struble, R. Hallgren, and U. L. Rohde, "A general noise de-embedding procedure for packaged two-port linear active devices," *IEEE Trans. Microw. Theory Tech.*, vol. 40, no. 11, pp. 2013–2024, Nov. 1992.
- [64] R. A. Pucel, H. Statz, and H. A. Haus, "Signal and Noise Properties of Gallium Arsenide Microwave Field-Effect Transistors," *Adv. Electron. Electron Phys.*, vol. 38, pp. 195–265, 1975.
- [65] L. Pfeiffer, K. W. West, H. L. Stormer, and K. W. Baldwin, "Electron mobilities exceeding  $10^7$  cm<sup>2</sup>/v s in modulation-doped GaAs," *Appl. Phys. Lett.*, vol. 55, no. 18, pp. 1888–1890, Oct. 1989.
- [66] I. Khalil, A. Liero, M. Rudolph, R. Lossy, and W. Heinrich, "GaN HEMT Potential for Low-Noise Highly Linear RF Applications," *IEEE Microw. Wireless Compon. Lett.*, vol. 18, no. 9, pp. 605–607, Sep. 2008.
- [67] E. M. Suijker, M. Rodenburg, J. A. Hoogland, M. van Heijningen, M. Seelmann-Eggebert, R. Quay, P. Bruckner, and F. E. van Vliet, "Robust AlGaIn/GaN Low Noise Amplifier MMICs for C-, Ku- and Ka-Band Space Applications," in *IEEE Compound Semiconductor Integrated Circuit Symposium, 2009*, Oct. 2009, pp. 1–4.
- [68] C. Trantanella, M. Pollman, and M. Shifrin, "An investigation of GaAs MMIC high power limiters for circuit protection," in *IEEE MTT-S Int. Microw. Symp. Dig.*, vol. 2, Jun. 1997, pp. 535–538.
- [69] A. P. M. Maas, J. P. B. Janssen, and F. E. van Vliet, "Set of X-band distributed absorptive limiter GaAs MMICs," in *2007 European Radar Conference*, Oct. 2007, pp. 17–20.
- [70] P. Schuh, H. Sledzik, R. Reber, K. Widmer, A. Fleckenstein, B. Schweizer, and M. Oppermann, "T/R-module technologies today and future trends," in *Proc. 40th Eur. Microw. Conf.*, Sep. 2010, pp. 1540–1543.
- [71] V. Alleva, A. Bettidi, A. Cetronio, M. De Dominicis, M. Ferrari, E. Giovine, C. Lanzierf, E. Limiti, A. Megna, M. Peroni, and P. Romanini, "High Power Microstrip GaN-HEMT Switches for Microwave Applications," in *European Microwave Integrated Circuit Conference*, Oct. 2008, pp. 194–197.
- [72] C. F. Campbell and D. C. Dumka, "Wideband high power GaN on SiC SPDT switch MMICs," in *IEEE MTT-S Int. Microw. Symp. Dig.*, May 2010, pp. 145–148.
- [73] A. Bettidi, A. Cetronio, M. Cicolani, C. Costrini, C. Lanzieri, S. Maccaconi, L. Marescialli, M. Peroni, and P. Romanini, "X-band T/R module in state-of-the-art GaN technology," in *Proc. Eur. Radar Conf.*, Oct. 2009, pp. 258–261.

- [74] M. I. Skolnik, *Radar Handbook*. McGraw-Hill Corp., 2008.
- [75] I. J. Bahl, “10W CW broadband balanced limiter/LNA fabricated using MSAG MESFET process,” *Int. J. RF Microw. Comput.-Aided Eng.*, vol. 13, no. 2, pp. 118–127, Mar. 2003.
- [76] T. Van den Broeck and J. Verspecht, “Calibrated vectorial nonlinear-network analyzers,” in *IEEE MTT-S Int. Microw. Symp. Dig.*, May 1994, pp. 1069–1072.
- [77] P. Blockley, D. Gunyan, and J. B. Scott, “Mixer-based, vector-corrected, vector signal/network analyzer offering 300kHz–20GHz bandwidth and traceable phase response,” in *IEEE MMT-S Int. Microw. Symp. Dig.*, Jun. 2005.
- [78] W. Van Moer and L. Gomme, “NVNA versus LSNA: enemies or friends?” *IEEE Microw. Mag.*, vol. 11, no. 1, pp. 97–103, Feb. 2010.
- [79] P. Wright, A. Sheikh, C. Roff, P. J. Tasker, and J. Benedikt, “Highly efficient operation modes in GaN power transistors delivering upwards of 81% efficiency and 12W output power,” in *IEEE MTT-S Int. Microw. Symp. Dig.*, Jun. 2008, pp. 1147–1150.
- [80] B. M. Green, V. Tilak, V. S. Kaper, J. A. Smart, J. R. Shealy, and L. F. Eastman, “Microwave power limits of AlGaIn/GaN HEMTs under pulsed-bias conditions,” *IEEE Trans. Microw. Theory Tech.*, vol. 51, no. 2, pp. 618–623, Feb. 2003.
- [81] F. H. Raab, “High-efficiency linear amplification by dynamic load modulation,” in *IEEE MTT-S Int. Microw. Symp. Dig.*, vol. 3, 2003, pp. 1717–1720.
- [82] J. M. Cusack, S. M. Perlow, and B. S. Perlman, “Automatic Load Contour Mapping for Microwave Power Transistors,” *IEEE Trans. Microw. Theory Tech.*, vol. 22, no. 12, pp. 1146–1152, Dec. 1974.
- [83] Y. Takayama, “A New Load-Pull Characterization Method for Microwave Power Transistors,” in *IEEE MTT-S Int. Microw. Symp. Dig.*, Jun. 1976, pp. 218–220.
- [84] G. P. Bava, U. Pisani, and V. Pozzolo, “Active load technique for load-pull characterisation at microwave frequencies,” *Electronics Letters*, vol. 18, no. 4, pp. 178–180, 18 1982.
- [85] M. S. Hashmi, A. L. Clarke, S. P. Woodington, J. Lees, J. Benedikt, and P. J. Tasker, “An Accurate Calibrate-Able Multiharmonic Active Load-Pull System Based on the Envelope Load-Pull Concept,” *IEEE Trans. Microw. Theory Tech.*, vol. 58, no. 3, pp. 656–664, Mar. 2010.
- [86] M. Squillante, M. Marchetti, M. Spirito, and L. C. N. de Vreede, “A mixed-signal approach for high-speed fully controlled multidimensional load-pull parameters sweep,” in *73rd Automat. RF Tech. Group Conf. Dig.*, Jun. 2009.

- [87] M. Marchetti, M. J. Pelk, K. Buisman, W. Neo, M. Spirito, and L. de Vreede, "Active Harmonic Load-Pull With Realistic Wideband Communications Signals," *IEEE Trans. Microw. Theory Tech.*, vol. 56, no. 12, pp. 2979–2988, Dec. 2008.
- [88] P. Poire, D.-L. Le, and F. Ghannouchi, "A PC controlled fully automatic active load-pull measurement system using a pseudo-gradient algorithm," *IEEE Instrum. Meas. Tech. Conf.*, pp. 628–631, Apr. 1995.
- [89] S. J. Doo, P. Roblin, V. Balasubramanian, R. Taylor, K. Dandu, J. Strahler, G. Jessen, and J.-P. Teyssier, "Pulsed Active Load-Pull Measurements for the Design of High-Efficiency Class-B RF Power Amplifiers With GaN HEMTs," *IEEE Trans. Microw. Theory Tech.*, vol. 57, no. 4, pp. 881–889, Apr. 2009.
- [90] ANTEVERTA microwave. [Online]. Available: <http://www.anteverta-mw.com/Single%20load%20and%20second>
- [91] M. Demmler, P. J. Tasker, M. Schlechtweg, and A. Huilsmann, "Direct extraction of non-linear intrinsic transistor behaviour from large signal waveform measurement data," in *Proc. 26th Eur. Microw. Conf.*, vol. 1, Sep. 1996, pp. 256–259.
- [92] H. Chireix, "High Power Outphasing Modulation," *Proc. IRE*, vol. 23, no. 11, pp. 1370–1392, 1935.
- [93] W. H. Doherty, "A New High Efficiency Power Amplifier for Modulated Waves," *Proc. IRE*, vol. 24, no. 9, pp. 1163–1182, 1936.
- [94] L. R. Kahn, "Single-Sideband Transmission by Envelope Elimination and Restoration," *Proc. IRE*, vol. 40, no. 7, pp. 803–806, 1952.
- [95] C. M. Andersson, N. Ejebjork, A. Henry, S. Andersson, E. Janzen, H. Zirath, and N. Rorsman, "A SiC Varactor With Large Effective Tuning Range for Microwave Power Applications," *IEEE Electron Device Lett.*, vol. 32, no. 6, pp. 788–790, Jun. 2011.
- [96] H. M. Nemati, H. Cao, B. Almgren, T. Eriksson, and C. Fager, "Design of Highly Efficient Load Modulation Transmitter for Wideband Cellular Applications," *IEEE Trans. Microw. Theory Tech.*, vol. 58, no. 11, pp. 2820–2828, Nov. 2010.
- [97] J. M. Manley and H. E. Rowe, "Some general properties of nonlinear elements-Part I. General energy relations," *Proc. IRE*, vol. 44, no. 7, pp. 904–913, 1956.
- [98] S. A. Maas, *Nonlinear microwave and RF circuits*. Artech House, Inc., 2003.
- [99] J. Verspecht, J. Horn, L. Betts, D. Gunyan, R. Pollard, C. Gillease, and D. E. Root, "Extension of X-parameters to include long-term dynamic memory effects," in *IEEE MTT-S Int. Microw. Symp. Dig.*, Jun. 2009, pp. 741–744.

- 
- [100] J. Schoukens, R. Pintelon, T. Dobrowiecki, and Y. Rolain, "Identification of linear systems with nonlinear distortions," *Automatica*, vol. 41, no. 3, pp. 491–504, 2005.
- [101] Y. Rolain, W. Van Moer, R. Pintelon, and J. Schoukens, "Experimental characterization of the nonlinear behavior of RF amplifiers," *IEEE Trans. Microwave Theory Tech.*, vol. 54, no. 8, pp. 3209–3218, 2006.
- [102] J. Schoukens and T. Dobrowiecki, "Design of broadband excitation signals with a user imposed power spectrum and amplitude distribution," in *IEEE Instrum. Meas. Technol. Conf.*, vol. 2, May 1998, pp. 1002–1005.



# Paper A

Electrothermal Access Resistance Model for GaN Based HEMTs

M. Thorsell, K. Andersson, H. Hjelmgren, and N. Rorsman

in *IEEE Transactions on Electron Devices*, vol. 58, no. 2, pp. 466–472, 2011



# Paper B

**Thermal Study of the High-Frequency Noise in GaN HEMTs**

**M. Thorsell, K. Andersson, M. Fagerlind, M. Südow, P.-Å. Nilsson,  
and N. Rorsman**

**in *IEEE Transactions on Microwave Theory and Techniques*, vol. 57,  
no. 1, pp. 19–26, 2009.**



# Paper C

**An X-Band AlGaN/GaN MMIC Receiver Front-End**

**M. Thorsell, M. Fagerlind, K. Andersson, N. Billström, and N. Rorsman**

**in *IEEE Microwave and Wireless Components Letters*, vol. 20, no. 1, pp. 55–57, 2010.**







# Paper D

**Fast Multi Harmonic Active Load-Pull System With Waveform Measurement Capabilities**

**M. Thorsell, and K. Andersson**

to appear in *IEEE Transactions on Microwave Theory and Techniques*



# Paper E

Characterization Setup for Device Level Dynamic Load Modulation Measurements

M. Thorsell, K. Andersson, and C. Fager

in *2009 IEEE MTT-S International Microwave Symposium Digest*, Boston, MA, USA, 2009.



# Paper F

**Extending the Best Linear Approximation to Characterize  
the Nonlinear Distortion in GaN HEMTs**

M. Thorsell, K. Andersson, G. Pailloncy, and Y. Rolain

to appear in *IEEE Transactions on Microwave Theory and Tech-  
niques*







# Paper G

**Nonlinear Characterization of Varactors for Tunable Networks by Active Source-Pull and Load-Pull**

**C. M. Andersson, M. Thorsell, and N. Rorsman**

**in *IEEE Transactions on Microwave Theory and Techniques*, vol. 59, no. 7, pp. 1753–1760, 2011**





